Preprint

Digital twins to quantify the impact of growing variability on the harvest quality of orange

Daniel Onwude[1*], Jade North[2], Paul Cronje[2], Rob Schouten[3], Thijs Defraeye[1,4]

[1]Empa, Swiss Federal Laboratories for Materials Science and Technology, Laboratory for Biomimetic Membranes and Textiles, Lerchenfeldstrasse 5, CH-9014 St. Gallen, Switzerland

[2]Citrus Research International, Department of Horticultural Science, University of Stellenbosch, Private Bag X1, Stellenbosch 7602, South Africa

[3] Wageningen Food and Biobased Research, Bornse Weilanden 9, 6708 WG Wageningen, the Netherlands

[4]Food Quality and Design, Wageningen University & Research, P.O. Box 17, 6700 AA Wageningen, the Netherlands

***** Corresponding author: daniel.onwude@empa.ch (D. Onwude) Empa, Swiss Federal Laboratories for Materials Science and Technology, Laboratory for Biomimetic Membranes and Textiles, Lerchenfeldstrasse 5, CH-9014 St. Gallen, Switzerland

ABSTRACT

The quality of citrus fruit is influenced by various growing conditions, including weather. However, the impact of weather differences between growing regions on citrus quality at harvest is not well understood. This study utilizes a mechanistic-driven digital replica of the growth process of a Valencia orange from fruit set until harvest to quantify this impact. The temperature, humidity, rainfall, and vapor pressure deficit data from different orange growing regions of South Africa, including Citrusdal, Nelspruit, Letsitele, and Sundays River Valley (SRV), are compared. The results suggest that the differences in weather conditions between growing regions affect fruit diameter (FD), fruit weight (FW), rind thickness (RT), rind weight (RW), total soluble solids (TSS), and titratable acidity (TA) of oranges at harvest. The differences between growing regions led to variations of up to threefold for FD, twofold for FW, RT, RW, TSS, and up to fourfold for TA upon harvest. Notably, oranges produced from warmer Letsitele and Nelspruit regions are found to be larger and less acidic compared to those from coastal SRV upon harvest. The study also reveals the impact of the fruit growth process on the temperature gradient within the fruit, which varies across growing regions. The maximal temperature difference between the fruit core and surface during the growth process ranges from ~2 °C to ~3 °C. These variations in fruit temperature gradient could lead to variations in temperature-driven quality decay of fruit from different climatic regions at the start of their postharvest journey. These findings provide valuable insights for the citrus industry, optimizing practices, harvest planning, and postharvest logistics. The output of this digital twin will help identify areas needing extra precooling to extend shelf life and minimize quality decay. Real-world use allows growers to schedule harvests based on regional weather conditions.

Keywords: Resource conservation; horticulture; virtual replica; cultural practices; citrus fruit; food waste

NOMENCLATURE

Symbols

ρ_i	Density (kg m^{-3})
C_{pi}	Specific heat capacity (J kg^{-1} K^{-1})
k_{i}	Thermal conductivity (W m^{-1} K^{-1})
$Q_{\mathrm{resp,i}}$	Volumetric heat of respiration (W m^{-3})
∇	Spatial derivative operator (-)
T_i	Fruit temperature (K)
i	Fruit pulp and rind domain
$\boldsymbol{n}$	Unit vector normal to the surface (-)

Q_o	Convective heat flux at the air-fruit interface (W m^{-2})
Q_R	Radiative heat flux (W m^{-2})
Q_E	Transpirational heat flux (W m^{-2})
k_t	Convective mass transfer coefficient (s m^{-1})
$P_{v,rind}$	Vapor pressure on the fruit surface (Pa)
$P_{v,air}$	Ambient vapor pressure (Pa)
P_{sat}	Saturated pressure (Pa)
a_w	Water activity below the fruit surface (-)
RH_{ave}	Average relative humidity (%)
h_c	Convective heat transfer coefficient (W m^{-2} K^{-1})
T_{air}	Air temperature (°C)
$T_{air,ave}$	Average daily air temperature during plant growth process (°C)
k_{air}	Thermal conductivity of air (W m^{-1} K^{-1})
U_{speed}	Wind speed (m s^{-1})
G_r	Grashof number (-)
ΔT	Temperature difference between fruit surface and air (°C)
β	Air volume expansion coefficient (K^{-1})
a_{sw}	Reflectance of orange rind to short-wave radiation
R_{sw}	Short-wave radiation received by the fruit (W m^{-2})
ε	Emissivity of infrared radiation for orange
R_{lw}	Long-wave radiation received by the fruit (W m^{-2})
σ	Stefan-Boltzmann radiation constant
$C_{p,pulp}$	Specific heat capacity of orange pulp (J kg^{-1} K^{-1})
$C_{p,rind}$	Specific heat capacity of orange rind (J kg^{-1} K^{-1})
ρ_{pulp}	Density of orange pulp (kg m^{-3})
ρ_{rind}	Density of orange rind (kg m^{-3})
k_{pulp}	Thermal conductivity of the orange pulp (W m^{-1} K^{-1})
k_{rind}	Thermal conductivity of the orange rind (W m^{-1} K^{-1})
MC	Moisture content of the material (%)

MC_{pulp}	Moisture content of the orange pulp (%),
MC_{rind}	Moisture content of the orange rind (%)
rfruit0	Initial fruit radius (mm)
r_{pulp}	Radius of pulp (mm)
r_{rind}	Radius of rind (mm)
$rind_{thick}$	Rind thickness (mm)
Nu	Nusselt number (-)
Re	Reynolds number (-)
ν_{air}	Kinematic viscosity of air ($m^2\ s^{-1}$)
Pr	Prandtl number for air (-)
μ_{air}	Absolute viscosity of air ($kg\ m^{-1}\ s^{-1}$)
$\mu_{air,\ rind}$	Viscosity of air at the fruit surface ($kg\ m^{-1}\ s^{-1}$)
Sc	Schmidt number (-)
$\delta_{wv,air}$	Diffusion coefficient of water vapor in the air ($m^2\ s^{-1}$)
T_{rind}	Surface/rind temperature (°C)
T	Temperature (°C)
RH_{air}	Relative humidity of the air (%)
$rind_{thick,0}$	Initial rind thickness (mm)
$r_{pulp,0}$	Initial pulp radius (mm)
T_{max}	Daily maximum temperature (˚C)
T_{min}	Daily minimum temperature (˚C)
T_b	Minimum temperature for crop growth (˚C)
t	Time (s)
RH	Relative humidity (%)
a_1	Crop growth parameter 1 for EPIC model
a_2	Crop growth parameter 2 for EPIC model
REG_k	Minimum crop stress factor on day k
FW_{max}	Maximum fruit weight (kg)
HUI_k	heat unit index on day k (0-1)
HUF_k	Heat unit factor on day k

FW_k	Fruit weight on day k (g)
WS_k	Water stress factor on day k (0-1)
TS_k	Plant temperature stress factor on day k
$u_{k,l}$	Water use in layer l on day k
EP_k	Potential plant water use on day k
T_{gr}	Average daily soil surface temperature per region r (°C)
T_{0r}	Optimal crop temperature per region r (°C)
$T_{ini,r}$	Initial crop temperature per region r (°C)
R^2	Coefficient of determination
RMSE	Root mean square error

Abbreviations/ Acronym

FW	Fruit weight (g)
FD	Fruit diameter (mm)
RW	Rind weight (g)
RT	Rind thickness (mm)
TSS	Total soluble solids (°Brix)
TA	Titratable acidity (%)
RP	Heat of respiration (W kg^{-1})
IQR	interquartile range
SRV	Sundays River Valley
EPIC	Environment, Plant, Interactions, and Control crop growth model
LINTUL	Light Nutrient and Temperature crop growth model
SUCROS	SUrface CROp System model
WOFOST	World Food Studies crop growth simulation model
SIMPLE	Simple generic crop model
MUMPS	MUltifrontal Massively Parallel sparse direct Solver
VPD	Vapor Pressure Deficit (kPa)
HU	Heat Units (°C)
HUI	Heat unit index (0-1)

PHU	Potential heat unit for crop maturation (°C)
HUF	Heat unit factor (0-1)

1. INTRODUCTION

Citrus is one of the most cultivated fruit crops in the world and is grown in more than 80 countries, mostly under tropical and sub-tropical climates [1]. They are known for their thirst-quenching ability, refreshing fragrance, and abundant vitamin C content [2, 3]. However, differences in their growing conditions can affect the quality of oranges at harvest [4–6].

The fruit growth and physiological quality properties of oranges often depend on several pre-harvest factors, such as horticultural practices, and climatic variability [7]. However, weather conditions have the most predominant effect on fruit growth and quality [8]. A suitable growth temperature is a critical factor for successful citrus production, with optimal growth conditions between 13 and 32 °C. On the one hand, a very high temperature reduces fruit growth by decreasing total tree CO_2 assimilation and increasing fruit drop [9]. Internal fruit quality parameters, such as sugar and acid contents, are also affected [10]. On the other hand, too low temperature results in frosts and freezing damage to fruit tissue [9]. Additionally, moisture stress during fruit formation and development also affect fruit quality [11]. All these make that the differences in weather conditions between citrus growing regions affect fruit quality (e.g., fruit size and sugar content) at harvest. Therefore, it is essential to comprehend the impact of these climatic differences on orange production to better understand the development of citrus quality. One approach to achieving this is by predicting how fruit quality evolves during growth and development under different growing conditions.

Crop growth models have been explored to describe the growth and development of plants under different growing conditions. For this purpose, mechanistic and empirical models such as LINTUL [12], SUCROS [12],WOFOST [13], SIMPLE [14], von Bertalanffy [15, 16], and EPIC [17] have largely been deployed to predict the growth of fruits and vegetables in the past decades. However, relatively few studies explicitly modeled the impact of growing conditions, such as weather variability, on citrus fruit quality at harvest [18]. Rarely is the effect of the variability in weather conditions on multiple physiochemical properties of fruit upon harvest accounted for.

To bridge this gap, we have pioneered a novel approach by creating a virtual model of oranges that encompasses their growth cycle from fruit set until harvest. This virtual modeling approach is commonly referred to as a digital twin or digital shadow. Our digital twin of oranges, from fruit set until harvest, is a virtual model that replicates the key characteristics of oranges in a computer-based environment. This model incorporates essential fruit properties and simulates a wide range of physiological, metabolic, and thermal processes that occur during the growth and development of oranges. It is also linked to real-world processes through sensor data [4, 19]. Using this approach, we evaluate the impact of climatic variability between growing regions on the quality of oranges upon harvest. Our study includes metrics such as fruit weight (FW), fruit diameter (FD), rind thickness (RT), rind weight (RW), total soluble solids (TSS), and total titratable acidity (TA). We also simulate the physics-based thermal stress experienced by fruit as it grows. This allows us to ascertain the temperature gradient of the fruit at the time of harvest, a crucial factor influencing the postharvest longevity of the fruits.

2. MATERIALS AND METHODS

2.1 Study area

This study considered 'Turkey' Valencia oranges produced over the 2018/2019 season during the generic fruit growth stages phase I (1 September – 31 December), II (1 January – 15 May) and III (16 May – 31 July/August). Four major citrus growing regions of South Africa (SA) with distinctly different climate zones (Figure 1) were used for data collection. These areas are Letsitele in Limpopo, Nelspruit in Mpumalanga, Sundays River Valley (SRV) in Eastern Cape, and Citrusdal in Western Cape. More details of the production information of the experimental sites can be found in Table S1 in the supplementary material.

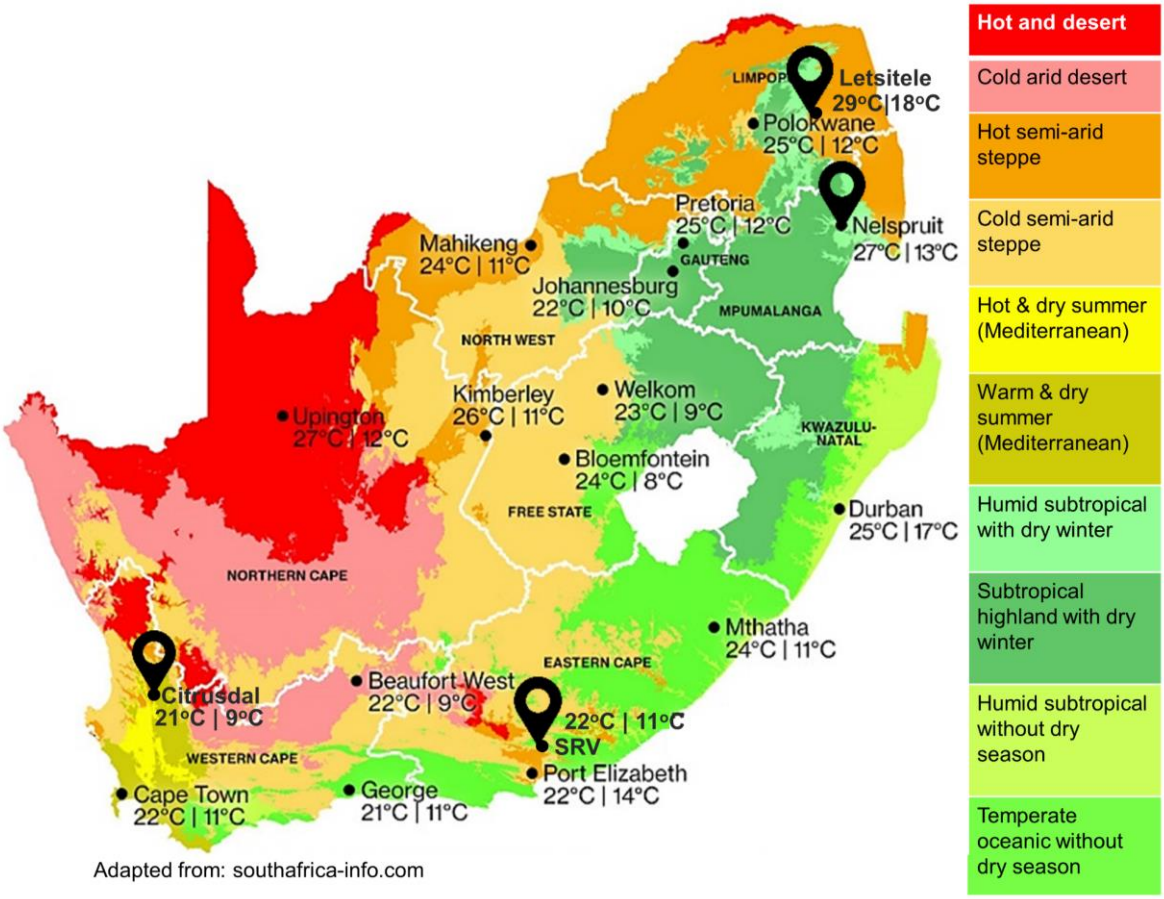

Figure 1. Map of several climate zones and the four major citrus-growing regions within South Africa, with indicated annual maximum and minimum temperatures [20].

2.2 Experimental Measurement

2.2.1 Growing regions and fruit sampling

We examined 'Turkey' Valencia oranges grown in the four regions, as Valencia is the most produced orange cultivar in South Africa, accounting for 44% of citrus exports from southern Africa [21]. 'Turkey' is one of the first Valencia cultivars to mature and is harvested between the last week of May and June in warmer climates. For this study, we

harvested orange fruit from five commercial orchards in each region. Ten adjacent trees that were uniform in size and vigor were selected and tagged within each orchard, and these trees were reserved for harvesting (Table S1). Fifteen fruit per tree were harvested from the outside up to 30 cm into the canopy to obtain 150 fruit per orchard. All fruit were harvested at commercial harvesting maturity as determined by the citrus producers per region; therefore, the harvesting times differed between regions.

2.2.2 External and internal fruit quality evaluation

The external fruit quality, such as fruit total weight (g) and rind weight (g) of each orange fruit at harvest, was determined using an electronic scale NBK-30 (Model NWH 10422, UWE South Africa). The fruit size (mm) and rind thickness (mm) were measured using a caliper (CD-6" C, Mitutoyo Corp, Tokyo, Japan).

The internal quality of the fruit at harvest was assessed by cutting along the longitudinal plane of the fruit for juice extraction using a citrus juicer (8-SA10, Sunkist®, Chicago, USA). Pulp particles were removed from the juice by straining through a muslin cloth to produce a pure citrus juice sample for each replicate. Titratable acidity (TA) was determined by titrating 20 ml of juice against 0.1562 N sodium hydroxide. Phenolphthalein was used as an indicator and titration was complete when the liquid turned pink in color. Data was expressed as a percentage citric acid content. The total soluble solids (TSS) of the fruit pulp (measured as °Brix and expressed as % TSS in the pulp) was determined using a digital refractometer (PR-32 Palette, ATAGO CO, Tokyo, Japan) (North-Dewing, 2023).

2.2.3 Weather data

Weather data per region from August 2018 to September 2019, covering the entire fruit development period, were obtained using the Agricultural Research Council (ARC) automated weather stations. Daily minimum and maximum temperature (°C), minimum and maximum relative humidity (% RH), and rainfall (mm) data were obtained. We also collected wind speed (U_{speed}, m s^{-1}), short-wave (W m^{-2}) and long-wave (W m^{-2}) radiation data during the growth process for these locations from NASA, via https://power.larc.nasa.gov/data-access-viewer/. Table 1 presents the selected weather differences between the four major citrus-growing areas of South Africa.

We also estimated the vapor pressure deficit (VPD), which is a measure of the difference between the amount of moisture in the air and the maximum amount of moisture the air can hold when it is saturated at a given temperature. VPD (kPa) was derived from temperature and humidity parameters using the following calculation (Equation 1) [22]:

$$\text{VPD} = 610.78\text{e}^{\left(\frac{\text{T}}{T+23.3}x17.27\right)}x\ \left(1-\frac{RH}{100}\right) \quad (1)$$

where T is the average temperature [((Maximum + Minimum)/2) (°C)], and RH is the average relative humidity [((Maximum + Minimum)/2) (%)].

Heat units are frequently used to describe the timing of biological processes, assuming no other limiting factors such as water and nutrition stress exist [23]. According to [23], HU (°C) is a useful tool for assessing the suitability of a region for growing citrus, as well as for estimating the duration of different growth stages and predicting the time of fruit maturation.

Heat Units (HU) were calculated for each day (i) per region using the following formula (Equation 2) [23]:

$$\text{HU}_i = \left(\frac{T_{max}+T_{min}}{2}\right) - T_b \quad (2)$$

where T_{max} is the daily maximum temperature, T_{min} is the minimum daily temperature, and T_b is the minimum temperature to sustain growth (for citrus, $T_b = 13\ °C$).

Table 1. Differences in weather conditions between the four different growing regions for the 2018/2019 season during fruit growth stages phase I (1 Sept. – 31 Dec.), II (1 Jan. – 15 May) and III (16 May – Jul./31 Aug.). Temperature, RH and VPD were calculated by averaging the daily values over the growth phase.

Growing regions	Fruit growth stages	Maximum temperature (°C)	Minimum temperature (°C)	Maximum RH (%)	Minimum RH (%)	Rain (mm)	VPD (kPa)
Nelspruit	I	33.4	17.4	84.4	33.1	153.4	1.6
	II	32.9	20.5	88.2	45.6	318.8	1.1
	III	28.5*	12.2*	83.5*	33.8*	1.5*	1.0*
Citrusdal	I	29.8	10.1	89.4	25.0	70.0	1.5
	II	31.9	13.1	90.7	26.1	43.8	1.5
	III	22.5	4.3	98.8	36.2	190.3	0.5
SRV	I	29.5	11.5	90.6	30.9	71.4	1.1
	II	31.2	15.3	90.4	37.8	97.0	1.1
	III	27.0	6.1	89.9	26.9	16.0	0.9
Letsitele	I	32.5	16.3	81.4	28.4	7.4	1.6
	II	31.9	19.1	89.7	41.0	4.4	1.1
	III	28.3*	8.7*	87.1*	24.3*	1.6*	1.1*

* Data until July 2019.

2.3 Digital twin configuration of a fruit

We created digital twins of 'Valencia' oranges to quantify the impact of weather conditions of citrus growing regions on the fruit quality during growth. We modeled a single fruit as a two-dimensional axisymmetric geometry of a sphere (Figure 2). The domain was divided into two sections of the fruit – the rind (initial thickness ($r_{ind-thick,0}$) = 1.8 mm) and the fruit pulp (initial pulp radius ($r_{pulp,0}$) = 2.5 mm). The initial values are based on the experimental data of Valencia orange from the literature [24, 25]. Using the EPIC crop growth model, we first simulated the daily fruit weight over time based on heat unit (HU) and maximum fruit weight value from fruit set until harvest. The EPIC model was calibrated with real data and linked to daily weather data during the growing season obtained using automated weather stations (see section 2.2.3). The EPIC model can simulate several fruit using unique input parameter values for each fruit. This mechanistic model can also simulate the growth process for both annual and perennial crops under varying environmental conditions [26, 27]. Other fruit quality parameters, including fruit diameter, rind thickness, rind weight, total soluble solids, and titratable acidity, were modeled using empirical regression models based on daily potential fruit weight (see section 2.4). We then used the finite element method to simulate

the physics-driven thermal stress of fruit during the growth process to determine the fruit temperature. Using this digital twin, we quantified the impact of growth conditions between the four regions on fruit quality at harvest.

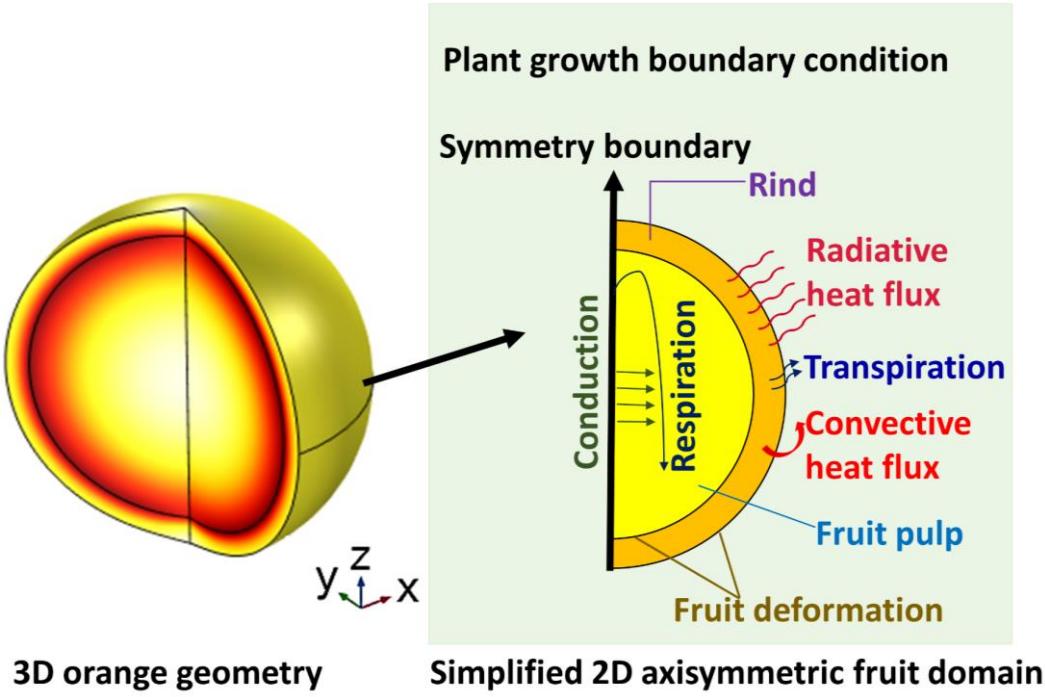

Figure 2. Geometry and boundary conditions of orange during the plant growth process (figure not to scale).

2.4 Mechanistic model for pre-harvest fruit growth process

A mechanistic model was developed to predict the fruit growth process, internal and external fruit quality at harvest, and the fruit temperature evolution. This model couples several empirical functions with physics-based models. Additionally, empirical regression models were incorporated to predict FD, RW, RT, TSS, and TA based on the predicted FW using the EPIC model. Figure 3 illustrates a flow chart outlining the methodology for creating a digital twin of oranges grown in various regions of South Africa, spanning from fruit set to harvest.

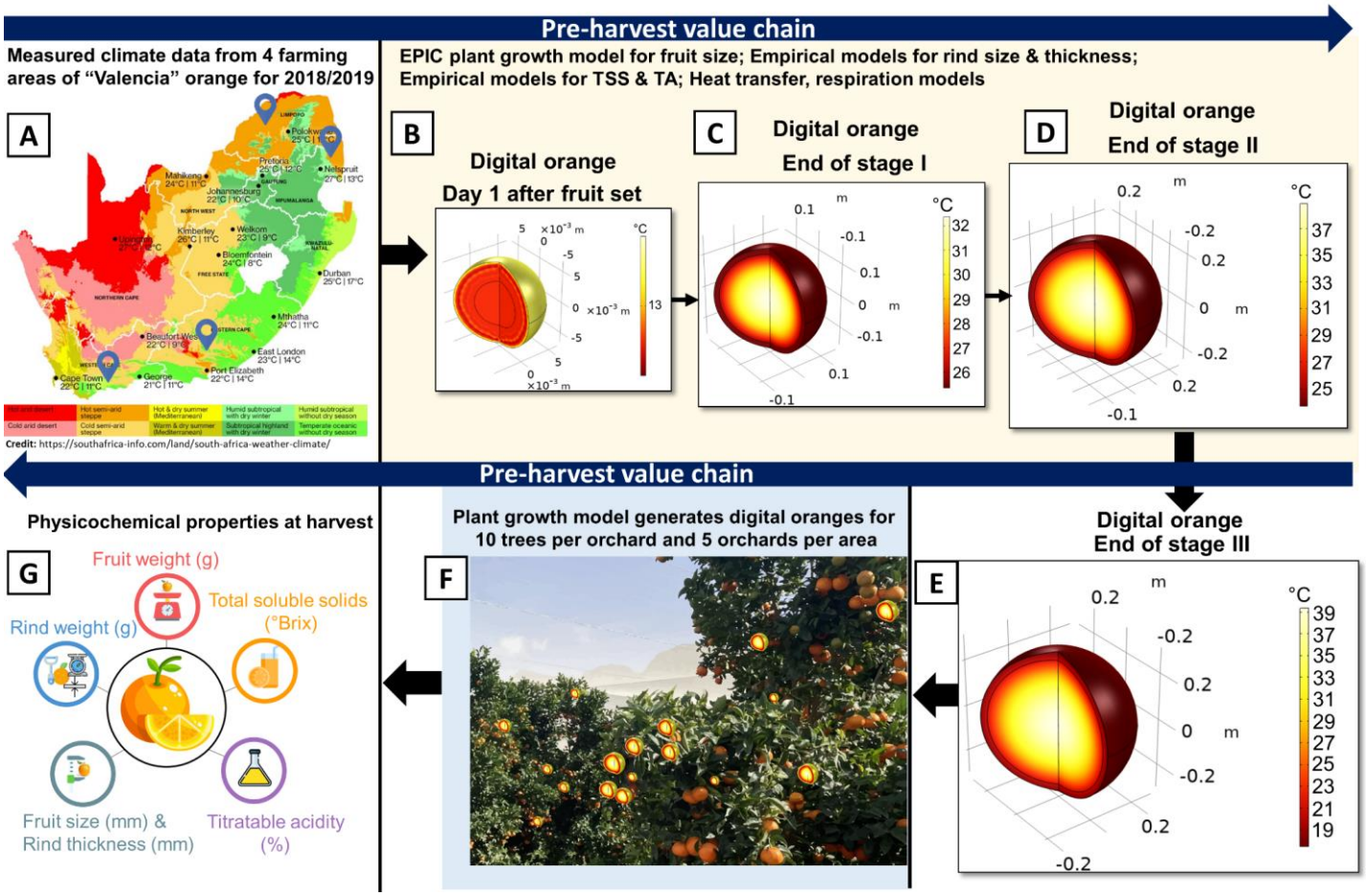

Figure 3. A flowchart of the overall methodology implemented from weather data collection to the fruit quality at harvest (figure not to scale).

2.4.1 EPIC crop growth model

The EPIC crop model is based mainly on a collection of empirical functions for various plant growth processes [27]. These processes are mainly modeled based on potential biomass growth, nutrient absorption, water use, crop yield, and growth stress. This study used a modified EPIC model to simulate the fruit weight of a single Valencia orange on a daily scale [17]. The leaves, flower bud, and tree are not taken into account. We also assume uniform expansion on all fruit sides during growth.

The potential fruit growth depends on weather variables such as maximum and minimum daily temperature, and heat units of the previous day (Figure 3A). The fruit growth process is based on the daily heat unit calculated from Equation 2 [17, 23, 27].

Based on the effective heat unit values, we then calculate the heat unit index (HUI) with values ranging from 0 at the start of fruit set to 1 at physiological maturity (time to harvest) [17, 27]:

$$\mathrm{HUI}_k \frac{\sum_{i=1}^{k} \mathrm{HU}_i}{\mathrm{PHU}} \quad (3)$$

where HUI_k (0-1) is the heat unit index on day k and PHU is the potential heat unit for crop maturation. PHU (°C) is calculated based on the daily heat unit for a specific location and time period from fruit set to harvest (PHU = $\sum_{fruit\ set}^{harvest} \mathrm{HU}_i$)[17, 28]. The total duration from fruit set to harvest for oranges from Letsitele is 200 days, 193 days for Nelspruit, 235 days for Citrusdal and 214 days for SRV. Based on this and daily heat unit data, the PHU values for Valencia orange produced in Letsitele is 2559, 2557 for Nelspruit, that of Citrusdal is 16230 and SRV is 1918.

With Equation 3, we compute the heat unit factor (HUF) [17, 27]:

$$\mathrm{HUF}_k = \frac{\mathrm{HUI_k}}{\mathrm{HUI}_k + exp(a_1 - (a_2)(\mathrm{HUI}_k))} \quad (4)$$

where $a_1$and a_2 are two crop parameters calculated by solving Equation 4 simultaneously using two pairs of values for HUI and HUF. The values for $a_1$and a_2 in this study are 0.049 and 7.422, respectively. Note that a_1 governs how fast the crop biomass accumulates in the early stages after planting while a_2 influences how the growth rate slows down as the crop approaches its maximum potential biomass.

To predict the growth process of a single Valencia orange, we use a relation between heat unit, maximum fruit weight, and the minimum crop stress factor (REG) [17]:

$$\mathrm{FW}_k = \mathrm{FW}_{max}\sqrt{(\mathrm{HUF}_k)(\mathrm{REG}_k)} \quad (5)$$

where FW_k is the fruit weight on day k (kg), and FW_{max} is the maximum fruit weight (g). Using the experimental data of FW_{max} estimated over different growing season per region, we modeled the fruit growth process of 50 oranges from 10 trees in five orchards within a region to capture microclimate variability.

The crop growth stress factor, REG ranges from 0 to 1 and is the minimum stress factor between temperature and water stress, calibrated using experimental data.

Here, $\mathrm{REG}_k = min(\mathrm{WS}_k, \mathrm{TS}_k)$ (6)

where WS_k is the water stress factor given as [27]:

$$\mathrm{WS}_k = \frac{\sum_{l=1}^{M} u_{k,l}}{EP_k} \quad (7)$$

And TS_k is the plant temperature stress factor given as [27]:

$$TS_k = \sin\left(\frac{\pi}{2}\left(\frac{T_{gr} - T_b}{T_{0r} - T_b}\right)\right) \quad (8)$$

where u is the water use in a given soil layer l, and EP is the potential plant water use on day k, T_{gr} is the average daily soil surface temperature (°C) per growing region, and T_{0r} is the optimal crop temperature (23 °C) per region. For this study, T_{gr} was estimated from the Earth's skin temperature for 2018/2019 growing season per region obtained from NASA, via https://power.larc.nasa.gov/data-access-viewer/. The estimated average T_{gr} are 24.76 °C for Letsitele °C, 25.29 °C for Nelspruit, 18.52 °C for Citrusdal, and 20.38 °C for SRV. Note that TS_k = REG for this study as the values of $TS_k < \mathrm{WS}_k$.

As described in section 2.2, the collected weather and fruit weight data and other experimental data from the literature [24, 25] were used to calibrate the EPIC model. The literature data were extracted using WebPlotDigitizer 4.6. A graph of predicted fruit size with experimental fruit size data from the literature is shown in the supplementary data (Figure S1).

2.4.2 Empirical regression model for external and internal fruit parameters

In this study, the empirical regression functions used to model fruit diameter (mm), rind weight (g), rind thickness (mm), total soluble solids (°Brix TSS), and titratable acidity (% TA) upon harvest were selected based on the following features:

1. They are monotonic, i.e., they generate varying straight lines or curves that are always decreasing or increasing, consistent with the general knowledge of physiochemical fruit properties during growth and development.
2. The model consists of as few independent parameters as possible to describe the given data sets with acceptable accuracy.
3. The model-predicted data agree reasonably well with the experimental data.

Based on these features, polynomial, linear, power, logarithmic, piecewise and exponential functions were identified as likely to predict orange's external and internal qualities accurately during the growth process.

All the above models were fitted to data obtained from the literature using ORIGINPRO 2022 (64-bit) SR1 (Government) (OriginLab, Northampton, Massachusetts, USA). The performance of the models was evaluated by comparing the coefficient of determination (R^2) and the root mean square error (RMSE). Acceptable predictions were determined based on a criterion of a coefficient of determination (R^2) greater than or equal to 0.5, along with a minimized root mean square error (RMSE) [17, 29, 30]. The power function gave a reasonable prediction of fruit diameter (FD, mm) and rind weight (RW, g) during plant growth and are represented as:

$$FD = 6.7e^{FW^{0.167}} \qquad R^2 = 0.97;\ RMSE = 3.24 \qquad (9)$$

$$RW = 1.38e^{FW^{0.274}} \qquad R^2 = 0.74;\ RMSE = 5.77 \qquad (10)$$

The models were calibrated using growth data of 1067 Valencia oranges from two growing seasons in Gosford district of New South Wales [24]. The calibration plots are shown in the supplementary material (Figure S2-S3). Similar relationship between single fruit weight (FW) and fruit diameters (FD) or single fruit weight and rind weight (RW) for fruits and vegetables has also been reported in the literature [17, 31, 32]. It should be noted that the relationship between fruit weight (FW) and fruit diameter (FD) for 'Turkey' Valencia oranges may also be a polynomial. A curvilinear relationship could best explain this relationship, including quadratic, logarithmic or exponential. The relationship between FW and FD can be influenced by factors such as individual fruit variability, growing conditions, and maturity, which can affect the changes in fruit weight and size data. Therefore, using different empirical regression models to correlate FW and FD during growth for an cultivar, region, and even orchard would be the best approach to capture this variation. Unfortunately, such data are not available in the literature. Generally, as the fruit weight increases, the fruit diameter tends to increase until it reaches a maximum value before leveling off.

The rind thickness (RT, mm) for Valencia oranges has been shown to sometimes have a unimodal relationship with fruit size during the plant growth process [33, 34]. As the fruit grows, the rind begins to thicken, mainly due to the accumulation of cellulose and hemicellulose in the cell walls of the outermost layer of the fruit. However, as the fruit continues to grow and approaches maturity, the rind thickness may begin to decrease depending on the pulp juice accumluation. The rind can also maintain the thickness but will decrease as a percentage of the total fruit size as the fruit pulp expands during maturation. To capture this relationship, a piecewise empirical model based on fruit size (mm) was developed and calibrated with data from (see supplementary material for details-Figure S4) [33]. This model provided the most accurate representation of rind thickness compared to polynomial, power, logarithmic, and exponential functions:

$$\begin{cases} \mathrm{RT} = -2.7 + 0.134FD & (\mathrm{FD} < 55.48) \quad (11) \\ \mathrm{RT} = 4.44 + 0.143\,(FD - 55.48) & (55.48 < \mathrm{FD} < 59.92) \quad (12) \\ \mathrm{RT} = 5.07 - 0.050\,(FD - 59.92) & (\mathrm{FD} > 59.92) \quad (13) \end{cases}$$

$R^2 = 0.90$; RMSE = 0.00

The heat of respiration (RP) during plant growth and development was obtained from an exponential relationship with fruit weight (FW, kg) and calibrated (see Figure S5 for calibration plot) with data from [24]:

$$\mathrm{RP} = 0.15 + 0.54\exp^{(-FW/0.053)} \qquad R^2 = 0.99;\ \mathrm{RMSE} = 0.02 \qquad (14)$$

Similar to literature reports on other fruits [35, 36], polynomial models best explained the TSS quantified as °Brix and TA (%) of orange pulp during growth as expressed below:

$$\mathrm{TSS} = 15.02 - 0.048\mathrm{RP} + 1.2528E^{-4}RP^2 \qquad R^2 = 0.99;\ \mathrm{RMSE} = 0.17 \qquad (15)$$

$$\mathrm{TA} = 4.11 - 43.4\mathrm{RP} + 125.6RP^2 \qquad R^2 = 0.97;\ \mathrm{RMSE} = 0.18 \qquad (16)$$

where RP is the heat of respiration expressed in W kg^{-1}. The models were calibrated using citrus growth data of grapefruit [37]. The calibration plots are shown in the supplementary material (Figure S5 – S7). A curvilinear, polynomial pattern characterizes the relationship between TSS, TA, and respiration rate in Valencia oranges during growth. As the fruit matures, dynamic changes in TSS, TA, and respiration rate are observed, but these changes are inconsistent over time. Specifically, as the fruit grows, TSS increases while TA and respiration rate decrease until a point is reached where they level off.

2.4.3 Thermal model

Following the approach put forward by [38, 39], we solved the spatial and temporal heat load (thermal stress) variations on the fruit surface due to its interaction with the environment using the equation below. To reduce the complexity of the model, we simplify the system by assuming thermal equilibrium between all components and phases inside the fruit. In addition, we assumed heat loss from only respiration activity inside the fruit.

$$\rho_i C_{pi} \frac{\delta T_i}{\delta t} = Q_{resp,i} - \nabla \cdot (-k_i \nabla T_i) \quad (17)$$

ρ_i is the density (kg m^{-3}), $C_{p,i}$ is the specific heat capacity (J kg^{-1} K^{-1}), T_i is the fruit temperature (K), k_i is the thermal conductivity of the material (W m^{-1} K^{-1}), ∇ is the spatial derivative operator, and i represents the fruit pulp and rind domain. The material and thermal properties used in this study are given in Table 2. $Q_{resp,i}$ (W m^{-3}) represents the volumetric heat of respiration during plant growth. We calculated $Q_{resp,i}$ as a product of heat of respiration (RP, W kg^{-1}) and fruit pulp density ($\rho_{pulp,}$ kg m^{-3}).

The energy transferred through the boundary layer by conduction is carried away by convection through the air. We modeled the energy exchanges as boundary conditions by assuming that the normal heat flux at any point of the fruit surface was equal to the sum of sensible energy loss or gain by convection (Q_o), losss of energy by transpirational cooling (Q_E) and radiation (Q_R), taking into account the direction of heat flow along the surface normal:

$$n\,.(\mathrm{k}\nabla T) = Q_o + Q_E + Q_R \quad (18)$$

where n is the surface normal vector, i.e the vector that is perpendicular (normal) to the fruit surface at a specific point.

We indirectly modeled the convective heat flux (Q_o) between the fruit surface and the atmospheric air using the heat transfer coefficient as given below:

$$Q_o = h_c\left(T_{air,ave} - T_{rind}\right) \quad (19)$$

where Q_o is the convective heat flux at the air-fruit interface (W m^{-2}), h_c is the convective heat transfer coefficient (W m^{-2} K^{-1}), $T_{air,ave}$ is the average daily air temperature during plant growth process (K), and T_{rind} is the temperature at the fruit surface (K). The entire system (air and fruit domain) was assumed to be at an initial temperature for growth, $T_{ini,r}$ (26 °C) for Nelspruit, (24 °C) for Letsitele, (22 °C) for Citrusdal, and (27 °C) for SRV.

To estimate the spatially-varying convective heat transfer coefficient (h_c) over the fruit surface, we used an empirical relation of Nusselt number (Nu) for forced convection of a spherical shape as shown below [40, 41]:

$$Nu = \frac{h_c \mathrm{FD}}{k_{air}} = 2 + (0.4Re^{0.5} + 0.06Re^{0.667})Pr^{0.4}\left(\frac{\mu_{air}}{\mu_{air,rind}}\right)^{0.25} \quad (20)$$

where k_{air} is the thermal conductivity of air (= 0.0244 W m^{-1} K^{-1}), Re (=FD U_{speed}/υ_{air}) is the dimensionless Reynolds number as a function of the airspeed (-), Pr is the Prandtl number for air (= 0.73306).The values for μ_{air} and $\mu_{\mathrm{air,\ rind}}$ correspond respectively to the absolute viscosity of air (kg m^{-1} s^{-1}) and the viscosity of air at fruit surface (kg m^{-1} s^{-1}), which were considered to be equal, and υ_{air} is the kinematic viscosity of air (= 1.427E^{-5} m^2 s^{-1}).

Equation 20 is valid for only forced convection. In natural conditions, free and forced convection may occur. These types of convection measure the dynamics relationship of inertia (forced convection-Reynolds number) and buoyancy (free convection-Grashof number) to viscous forces in the fruit-air boundary layer. However, to further simplify our model, we determined the most dominant type of convective heat transfer on the fruit during growth and use only that for our simulation. To do this, we computed the ratio of the Grashof number (G_r) to the square of Reynolds

number (Re). According to [39, 42], forced convection dominates the heat transfer process when $G_r/Re^2 < 0.5$, while natural (or free) convection dominates when $G_r/Re^2 > 40$. In our study, $G_r/Re^2 < 0.05$. Therefore, buoyancy forces were neglected as forced convective heat transfer was dominant.

where $G_r(= 9.81\beta\Delta T\mathrm{FD}^3/\upsilon_{air})$ is the Grashof number (-), β $\left(= 2/\left(T_{rind} + T_{air,ave}\right)\right)$ is the air volume expansion coefficient (K^{-1}), and ΔT is the temperature difference between fruit surface and air (K),

Transpiration involves the evaporation of water from the surfaces of leaves and other aerial tree parts. This process leads to the cooling of the tree and its surroundings, including the fruits. As water evaporates from the surface of the fruit, it carries away heat, leading to cooling of the fruit. The transpiration heat flux (Q_E, $\mathrm{W\ m^{-2}}$) was modeled using the formula [39]:

$$Q_E = k_t \left(P_{v,rind} - P_{v,air}\right) \quad (21)$$

where k_t is the convective mass transfer coefficient ($\mathrm{s\ m^{-1}}$), $P_{v,rind}$, is the vapor pressure on the fruit surface (Pa) and $P_{v,air}$ is the ambient vapor pressure (Pa).

We determined k_t from the contribution of the resistance due to moisture migration through the rind (k_{rind}, $\mathrm{s\ m^{-1}}$) and the resistance to mass transfer due to the air boundary layer (k_{air} $\mathrm{s\ m^{-1}}$):

$$k_t = \left(\frac{1}{k_{air}} + \frac{1}{k_{rind}}\right)^{-1} \quad (22)$$

The air film mass transfer coefficient (k_{air}) was estimated based on the airspeed (u_{speed}, $\mathrm{m\ s^{-1}}$) using the Sherwood correlation for a sphere, as presented in Equation 7[43, 44].

$$Sh = \frac{k_{air}FD}{\delta_{wv,air}} = 2 + \ (0.552Re^{0.53}.\ Sc^{0.33}\ ) \quad (23)$$

where Sc ($=\upsilon_{air}\cdot\ \delta_{wv,air}{}^{-1}$) is the Schmidt number (-), $\delta_{wv,air}$ is the diffusion coefficient of water vapor in the air ($\mathrm{m^2\ s^{-1}}$).

The vapor pressure was dynamically linked with temperature using the Antoine equation [43], expressed as:

$$P_{sat} = \exp\left(23.4795 - \frac{3990.5}{T-39.317}\right) \quad (24)$$

Specifically, the vapor pressure just below the rind ($P_{v,rind,}$ Pa) was computed as follow:

$$P_{v,rind} = \ P_{sat}(T_{rind})\ x\ a_w \quad (25)$$

where P_{sat} is the saturated pressure (Pa) and a_w is the water activity below the fruit surface and was assume to be 1 (-).

While the vapor pressure of the air around the fruit ($P_{v,air}$, Pa) was estimated using the average relative humidity data during fruit growth (RH_{ave}, %):

$$P_{v,air} = \ RH_{ave}\ x\ P_{sat}\left(T_{air,ave}\right) \quad (26)$$

We modeled the radiative heat flux ($Q_R, W\ m^{-2}$) with the following equation [38]:

$$Q_R = (1 - a_{sw})R_{sw} + \varepsilon R_{lw} - \varepsilon\sigma T_{rind}^4 \quad (27)$$

To simplify the model, we assumed no radiation - radiation interaction between fruit due to direct exposure to sun-light. We also assumed isotropic radiation fields on the fruit surface during growth.

Here, a_{sw} is the reflectance of orange rind to short-wave radiation (= 0.63)[45, 46], R_{sw} is daily short-wave radiation received by the fruit (W m^{-2}) from fruit set until harvest per regions, ε is the emissivity of infrared radiation for orange (= 0.98)[47], R_{lw} is the daily long-wave radiation received by the fruit (W m^{-2}) from fruit set until harvest per regions, and σ is Stefan-Boltzmann radiation constant (= 5.67E^{-8} W m^{-2} K^{-4})[48].

Table 2. Material and thermal properties of orange fruit

Properties	***Domain***		***Reference***
Density (kg m^{-3})	Pulp	$\rho_{pulp} = \frac{FW-RW}{4.189*r_{pulp}^3}$	This study
	Rind	$\rho_{rind} = \frac{RW}{4.189*r_{rind}^3}$	
Specific heat capacity (J kg^{-1} K^{-1})	Pulp	$C_{p,pulp} = 1424.34 + 2673.19MC + 2.446T$	[49]
	Rind	$C_{p,rind} = 3300$	[4]
Thermal conductivity (W m^{-1} K^{-1})	Pulp	$k_{pulp} = 0.148 + 0.00493MC_{pulp}$	[50]
	Rind	$k_{rind} = 0.148 + 0.00493MC_{rind}$	[50]
Moisture content (%)	Fruit	$MC = 84.37 - 15.73\exp^{-0.009FW}$	[24]
	Pulp	$MC_{pulp} = 89.865 - 21.077\exp^{-0.00602FW}$	
	Rind	$MC_{rind} = 78.43 - 10.143\exp^{-0.0026FW}$	

Where ρ = Density of material [kg m^{-3}], ρ_{pulp} = Density of orange pulp [kg m^{-3}], ρ_{rind} = Density of orange rind [kg m^{-3}], $C_{p,pulp}$ = Specific heat capacity of orange pulp [J kg^{-1} K^{-1}], $C_{p,rind}$ = Specific heat capacity of orange rind [J kg^{-1} K^{-1}], k_{pulp} = Thermal conductivity of the orange pulp [W m^{-1} K^{-1}], k_{rind} = Thermal conductivity of the orange rind [W m^{-1} K^{-1}], MC = Moisture content of the material (%), MC_{pulp}= Moisture content of the orange pulp (%), MC_{rind} = Moisture content of the orange rind (%), T = Fruit temperature (K), FW = Fruit weight (kg), RW = Rind weight (kg), r_{pulp} = Radius of orange pulp (m), r_{rind} = Rind radius (RT + r_{pulp})(m), and RT = Rind thickness (m).

2.6 Numerical simulation

The pre-harvest semi-mechanistic model was implemented in COMSOL Multiphysics (version 6.1), a commercial finite element-based software. Using the linear interpolation function, we solved the single fruit growth model and external and internal fruit parameters (Eq. 3 – 16) (Figure 3B-G). To capture the looping of weather data as a function of time in the model, we used the "primitive relation function" under interpolation function for each day after fruit set. We simulated the transient conduction, radiative, and convective heat fluxes in the fruit during the growth process using the 'Bioheat Transfer' physics. As the boundary of the computational domain translates and deforms during the growth process, we modeled the uniform deformation using the "Deformed Geometry" physics and coupled it with

the heat transfer physics. We considered the fruit diameter change by integrating over the normal fruit displacement. The coupling was performed in a way such that the rind (FD/t) and pulp ((FD-RT)/t) domain velocities due to deformation are applied as the normal mesh velocities. A normal mesh was adopted for the simulation after mesh-sensitivity analysis (see supplementary material – Figure S10). We used parametric sweeps of transient studies to simulate 50 oranges from 10 trees in five orchards within a growing area (Figure 3F). Quadratic Lagrange geometry shape function, with automatic remeshing selection and a MUMPS (MUltifrontal Massively Parallel sparse direct Solver) fully-coupled direct solver was used for the simulation. The remeshing condition was set to "distortion" to reduce mesh distortion and enhance convergence. The relative tolerance was set to 10^{-7}, while 0.05 was the scaling factor. The time-stepping for the simulation was set to 86400 s, corresponding to the time interval of weather data recorded.

2.7 Statistical data analysis

To investigate the impact of climatic variability on the quality of oranges at harvest, a one-way analysis of variance (ANOVA) was performed. Prior to this, Levene's test was used to test the homogeneity of variance. Digital twin output for different growing regions was presented as median, 75th upper and 25th lower quartiles (box limits), and 1.5 × the interquartile range (IQR, whiskers) with a 0.95 confidence level. These statistical indicators were used to show the impact of climatic differences between growing areas on FW, FD, RW, RT, TSS and TA. We used Fisher LSD test at $p \leq 0.05$ significant level and 95% confidence interval to assess if there were significant differences in the fruit quality attributes within groups. We used the Tukey test to compare the simulated external and internal fruit quality data at harvest with the measured experimental data of the 2018/2019 season. Pearson's correlation coefficients (Pearson's r) at $p = 0.05$, 0.01, and 0.001 significant level was used to statistically determine the correlation between the fruit quality attributes and climatic parameters. We also performed a sensitivity analysis to assess the contribution of each model parameter to the variability of the different quality attributes at harvest. Equation 28 [51] was used for this sensitivity analysis. All analyses were conducted using ORIGINPRO 2022 (64-bit) SR1 (Government) (OriginLab, Northampton, Massachusetts, USA).

$$S = \frac{\partial x/x}{\partial p/p}\, x\, 100, \tag{28}$$

where S is the percentage scaled relative sensitivity, ∂x denotes the change in fruit quality parameter values, x represents the fruit quality parameter, p represents the model input parameters, and ∂p signifies the change in value for the model input parameters. These changes are considered at a ± 20% level on a temporal scale.

3. RESULTS AND DISCUSSION

3.1 Model verification for fruit quality parameters

We developed mechanistic and empirical models to predict the fruit weight (FW), fruit diameter (FD), rind weight (RW), rind thickness (RT), total soluble solids (TSS), and titratable acidity (TA) of oranges from different climatic regions at harvest. However, it is important to verify the accuracy of these models and evaluate their performance. We show in Figure 4 that the predicted fruit weight (Figure 4A) (using Eqn. 2 - 8) and diameter (Figure 4B) (using Eqn. 9) of Valencia orange for all growing regions agree reasonably well with that of our experimental data (max difference ≤ 25g for FW; max difference ≤ 2mm for FD) for the 2018/2019 growing season. The accuracy of the models is high, with an average difference of less than 15% between the predicted and experimental data across all growing

regions. This indicates that the models performed well in their ability to forecast outcomes accurately. Generally, the model verification demonstrates that the model effectively captures the impact of climatic variability among growing regions on fruit weight and size at harvest.

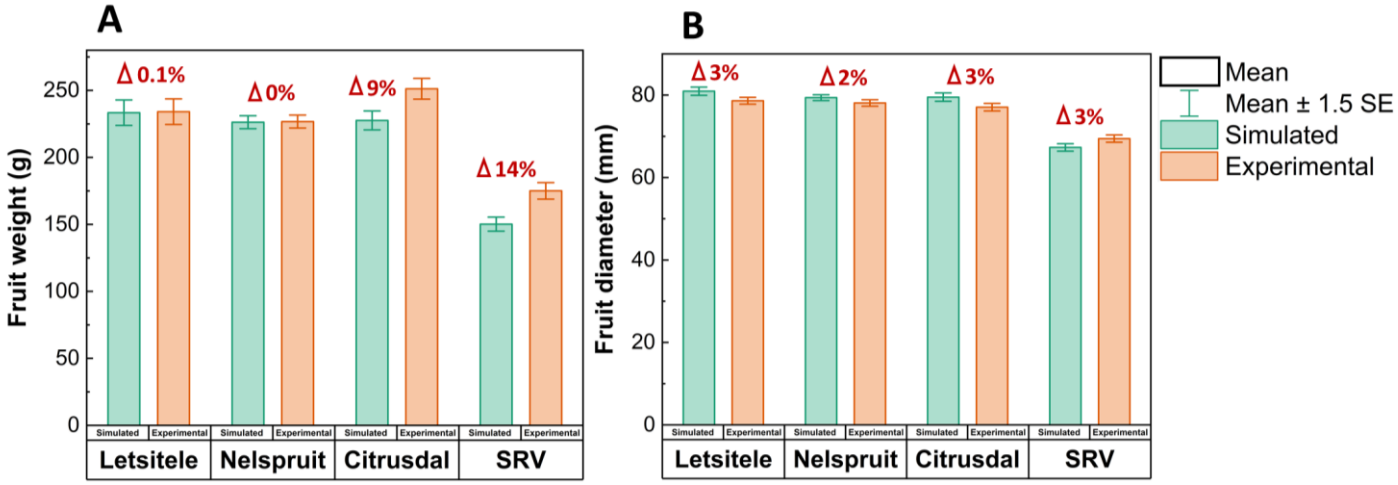

Figure 4. [A] Average experimental and digital twin simulated data of individual fruit weight (FW, g) for different growing regions at harvest; [B] Average experimental and digital twin simulated data of individual fruit diameter (FD, mm) for different growing regions at harvest. The error bar represent the mean ± 1.5 standard error. The percentage differences (Δ) between the experimental and simulated data for FW and FD are shown with the red-colored text.

Similarly, in Figure 5, it can be observed that the predicted values for rind weight (Figure 5A) (Eqn. 10), rind thickness (Figure 5B) (Eqn. 11-13), TA (Figure 5C) (Eqn. 14), and TSS (Figure 5D) (Eqn. 15) of Valencia orange are reasonably consistent with our experimental data across most regions. The differences between the predicted and experimental values are within acceptable ranges for Letsitele, Nelspruit, and SRV. The maximum variance of ≤ 10g for rind weight, ≤ 1.8mm for rind thickness, ≤ 0.6% for TA, and ≤ 2 °Brix for TSS are obtained. However, the largest disparities between our model-predicted data and the experimental results are found in Citrusdal data. Our model deviates by 25% for rind thickness, 20% for TSS and 40% for TA when compared to the experimental data for this growing region. These discrepancies can be attributed to substantial variations in weather patterns compared to the Letsitele, Nelspruit, and SRV regions. The calibration data used for our model, specifically the intermittent climate data from California for rind thickness [33] and the warmer climate data from Khartoum for TA and TSS [37], might have been insufficient to capture the complexities of the Mediterranean climate in Citrusdal. Additionally, the calibration data obtained from grapefruit for TA and TSS may not fully represent the unique characteristics of Citrusdal Valencia oranges. To address these issues and improve the accuracy of our model, it is crucial to calibrate the model using local quality data during the growth process from Citrusdal or nearby regions, particularly for Valencia oranges. Unfortunately, such data is currently unavailable, which poses a challenge. In addition, the harvesting conditions for our experiments slightly differ from that used for the modeling. This also could affect the accuracy of our model prediction. However, despite these limitations, the verification of our model demonstrates its effectiveness in capturing the influence of weather variability among different growing regions on rind weight, rind thickness, acidity, and total soluble solids at harvest.

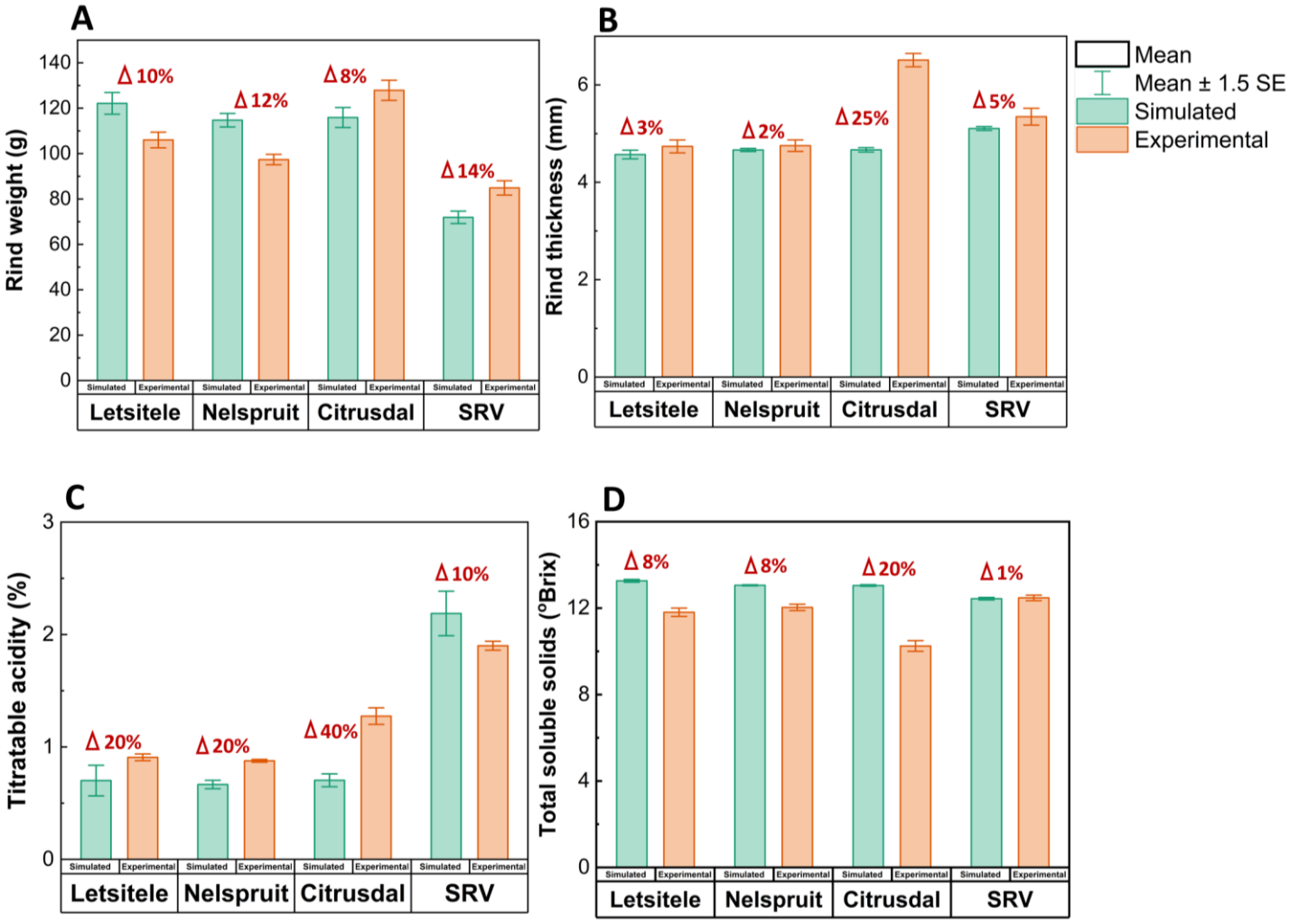

Figure 5. [A] Average experimental and digital twin simulated data of rind weight (g) for different growing regions at harvest; [B] Average experimental and digital twin simulated data of rind thickness (mm) for different growing regions; [C] Average experimental and digital twin simulated data of titratable acidity (%) for different growing regions; [D] Average experimental and digital twin simulated data of total soluble solids (° Brix) for different growing regions. The error bar represent the mean ± 1.5 standard error. The percentage differences (Δ) between the experimental and simulated data for RW, RT, TA and TSS are shown with the red-colored text.

3.2 Sensitivity analysis

We conducted an in-depth analysis to assess the influence of various model parameters on key fruit characteristics, including fruit diameter (FD), fruit weight (FW), rind thickness (RT), rind weight (RW), total soluble solids (TSS), total acidity (TA), and average fruit temperature at harvest. This sensitivity study is presented in Figure 6. Figure 6A highlights the influential model parameters contributing to the variability of FD, while Figure 6B focuses on the

sensitivity analysis of FW. For fruit diameter (Figure 6A), the most important parameters are optimal crop temperature (T_0) (22%), maximum fruit weight (FW_{max}) (20%), daily maximum temperature (T_{max}) (16%), daily minimum temperature (T_{min}) (15%), daily soil surface temperature (T_g) (15%), and minimum crop stress factor (REG) (11%). These parameters collectively accounted for the majority of the variability observed in FD. Conversely, the remaining parameters, including the minimum temperature for crop growth (T_b), crop growth parameter 2 (a_2), and potential heat unit for crop maturation (PHU), had a minimal impact, collectively contributing only 1% to the variability. Similarly, for fruit weight (Figure 6B), the most influential parameters are T_{max} (24%), T_{min} (22%), FW_{max} (17%), T_0 (16%), T_g (12%), and REG (8%). These parameters played significant roles in determining the variability of FW, while the remaining parameters (T_b, a_2, and PHU) collectively contributed 1% to the variability.

We observed that the impact of the variability in growing conditions on rind thickness at harvest is also largely sensitive to T_0 (34%), FW_{max} (25%), T_g (19%), REG (16%), T_{max} (2%), and T_{min} (2%) (Figure 6C). The remaining parameters (T_b, a_2, and PHU) collectively contributed ~2% to the variability. Our analysis indicated a similar trend for rind weight, with certain parameters demonstrating notable contributions (Figure 6D). FW_{max} had the largest impact, contributing 24% to the observed variability. T_0 closely followed, accounting for 21% of the variability. T_g, T_{max}, T_{min}, and REG also made significant contributions, with percentages of 16%, 14%, 13%, and 11%, respectively. The remaining parameters (T_b, a_2, and PHU) collectively contributed approximately 1% to the variability.

In relation to titratable acidity (Figure 6E) and total soluble solids (Figure 6F), our analysis reveals that T_0 has the most significant impact. T_0 contributes 59% to the observed variability in titratable acidity and 23% to the variability in total soluble solids. Following closely behind, FW_{max} accounts for 14% and 20% of the variability in acidity and total soluble solids, respectively. T_g, T_{max}, T_{min}, and REG collectively contribute to 26% of the observed variability for titratable acidity. On the other hand, total soluble solids are highly sensitive to these model parameters, collectively contributing 50% to the variability. The remaining parameters (T_b, a_2, and PHU) have a minimal impact, collectively accounting for only 1% of the variability in titratable acidity and total soluble solids.

Furthermore, we see that spatial-temporal temperature variations of Valencia orange in different growing regions are also highly sensitive to several growing environmental factors. Among these factors, T_{max} (41%), T_{min} (39%), daily long-wave radiation (R_{lw}) (10%), reflectance of orange rind to short-wave radiation (a_{sw}) (3%), daily short-wave radiation (R_{sw}) (2%), emissivity of infrared radiation (ε) (1%), and T_0 (1%) collectively contribute to 97% of the observed variability. On the other hand, factors such as FW_{max}, T_g, PHU, REG, equivalent fruit diameter (L_{eq}), a2, initial fruit radius (rfruit0), wind speed (U_{speed}), T_b, and crop growth parameter (a1) collectively account for 3% of the sensitivity of our model to spatial-temporal temperature variations during the growth process of oranges.

These findings emphasize the significance of specific parameters such as T_0, FW_{max}, T_{max}, T_{min}, T_g, and REG in accurately predicting the influence of growing conditions on fruit growth and quality of oranges. In addition to the temperature-related variables, radiation-related variables like daily long and short-wave radiation also play a crucial role in explaining the impact of growing conditions on variations in fruit temperature. These insights underscore the

importance of appropriately representing and incorporating these factors into our models to ensure reliable predictions. Moreover, this analysis provides actionable information that can be utilized to optimize fruit quality and enhance harvest outcomes. Growers can leverage this knowledge by making informed decisions and implementing targeted strategies to manipulate crop temperature, manage soil conditions, and mitigate stress factors. For example, adjusting orchard microclimates, irrigation practices, and canopy management techniques can help maintain optimal crop temperature, minimize stress, and promote desired fruit characteristics. Furthermore, citrus growers can utilize the model to predict and understand how changes in specific environmental factors may affect fruit quality. This knowledge empowers them to optimize their cultivation practices, tailor fertilization regimes, and make informed decisions regarding harvest timing and fruit processing.

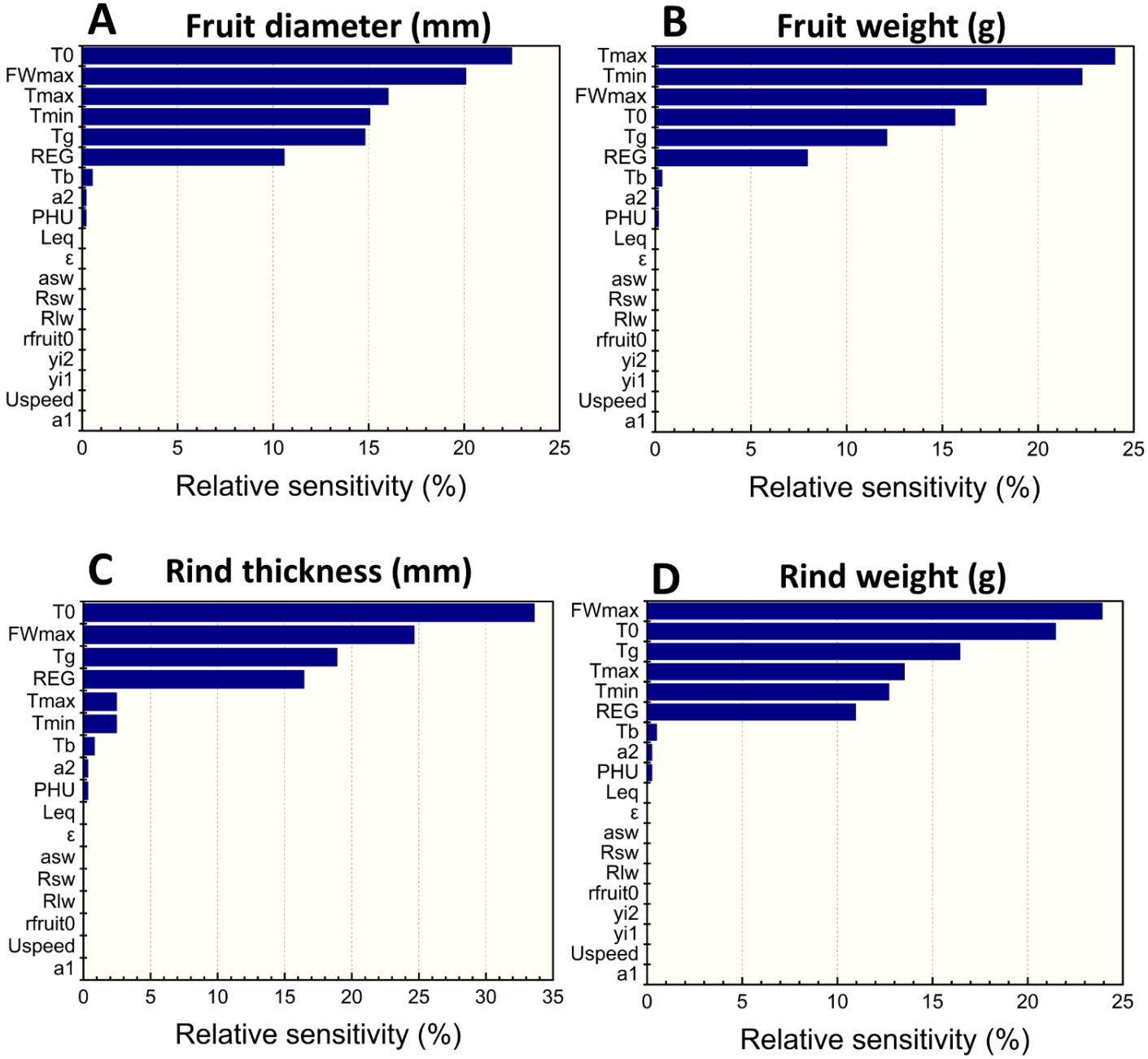

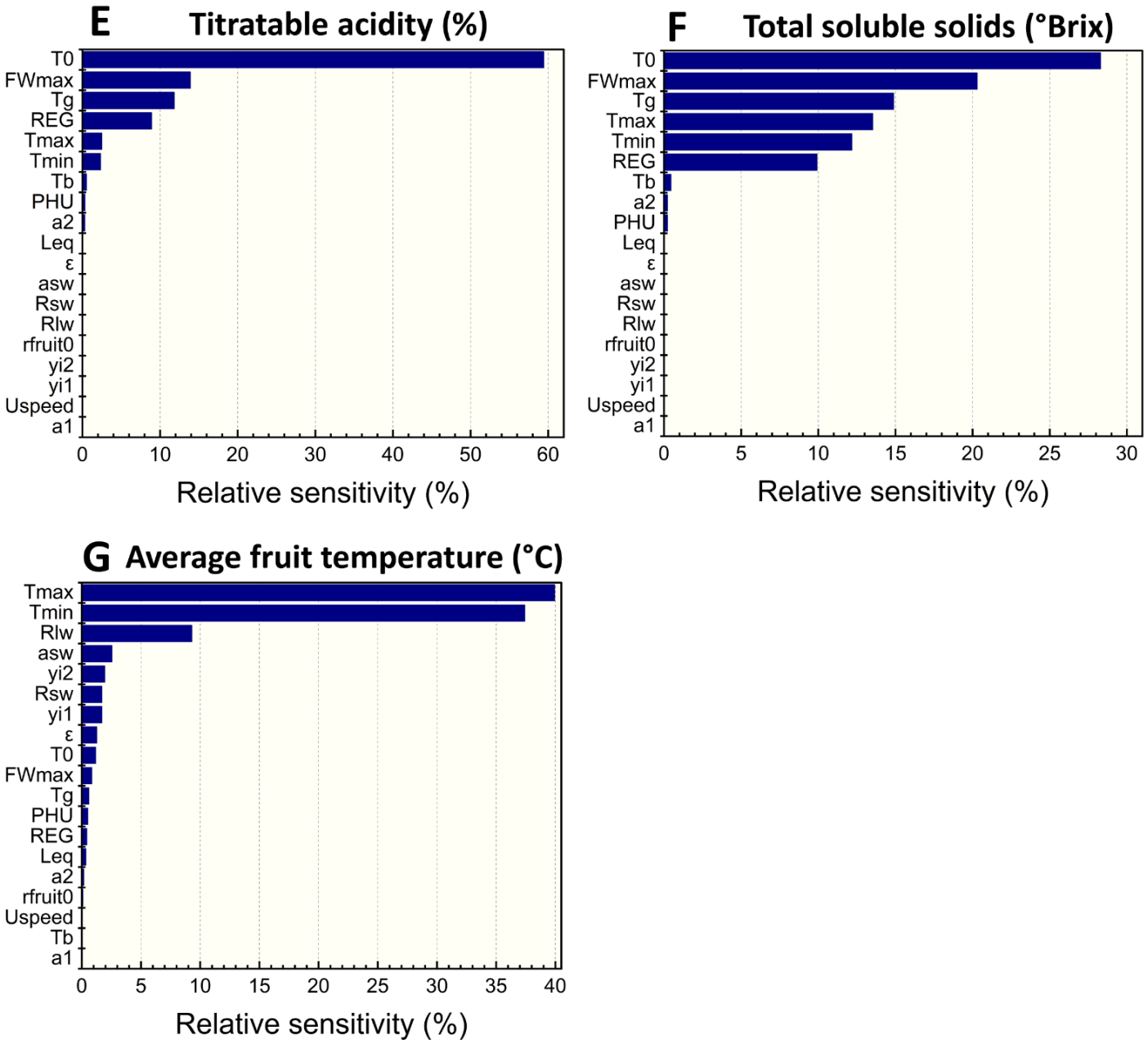

Figure 6. Impact of model parameters on (A) fruit diameter (mm), (B) fruit weight (g), (C) rind thickness (mm), (D) rind weight (g), (E) titratable acidity (%), (F) total soluble solids (°Brix), and (G) average volumetric fruit temperature (°C) of oranges at harvest. T_0 is optimal crop temperature, FW_{max} is maximum fruit weight, T_{max} is daily maximum temperature, T_{min} is daily minimum temperature, T_g is daily soil surface temperature, REG is a minimum crop stress factor, T_b is the minimum temperature for crop growth, a_1 and a_2 are crop growth parameters, PHU is potential heat unit for crop maturation, R_{lw} is daily long-wave radiation, R_{sw} is daily short-wave radiation, a_{sw} is reflectance of orange rind to short-wave radiation, ε is the emissivity of infrared radiation, L_{eq} is equivalent fruit diameter, rfruit0 is initial fruit radius, and U_{speed} is wind speed.

3.3 What is the impact of weather variation between growing regions on fruit quality attributes at harvest?

We evaluated the impact of weather variations between growing regions on fruit weight, fruit size, rind thickness, rind weight, total soluble solids (TSS), and titratable acidity (TA) of 'Turkey' Valencia oranges at harvest. Therefore, the various fruit quality output of our digital twin at harvest per growing region based on the coupled mechanistic and empirical models (Eqn. 3 – 17) were assessed (see section 2.6). Figure 7 illustrates the impact of the differences between growing regions on the external fruit quality parameters at harvest, so FW, FD, RW and RT. There is a significant effect of differences in growing regions on fruit weight (FW), fruit diameter (FD), rind thickness (RT), and rind weight (RW) at harvest. Oranges cultivated in the coastal SRV region exhibit lower fruit weight (Figure 7A), smaller fruit size (Figure 7B), thicker rind (Figure 7C), and lower rind weight (Figure 7D) compared to oranges grown in the Mediterranean Citrusdal region, as well as in the warmer climates of Letsitele and Nelspruit. The fruit size and weight of oranges from Nelspruit do not show a significant difference when compared to that from Letsitele. These findings align with our experimental results (results not shown).

For internal quality attributes, we showed the impact of weather variability between growing regions on titratable acidity (TA) and total soluble solids (TSS) of oranges at harvest (Figure 8). There is a significant impact of variations in growing regions on TA (Figure 8A) and TSS (Figure 8B) of oranges at harvest. The TA of oranges produced in SRV was significantly higher compared to those from Citrusdal, Letsitele, and Nelspruit (Figure 8A). However, the TSS were significantly lower (Figure 8B) in oranges from SRV. There were no significant differences in TA between oranges from Nelspruit and those from Letsitele and Citrusdal. The TSS of oranges grown in Nelspruit significantly differ from those grown in Citrusdal. This finding is consistent with our experimental results. Note that our model's TA prediction deviates largely from our experimental data in several regions (refer to Figure 5D). Consequently, the interaction between other growing regions for experimental data will differ from our model's prediction. Nevertheless, the variations in internal fruit quality at harvest are significantly influenced by the contrasting growth conditions among the orange growing regions.

Taking together, the oranges produced from Letsitele, and Nelspruit are larger with lower acidity compared to those from SRV. This could be because Letsitele and Nelspruit have higher average growing temperatures and heat units compared to those of SRV. Oranges thrive in moderately hot, sunny, dry and humid conditions, and as such, they tend to grow better in climates with higher average temperatures and effective heat units [18]. In addition, during stages I and II, which encompass early fruit growth and cell division, the size of the fruit is primarily determined. In warmer climates, the conducive optimum temperatures (see Figure 6A and B) during these stages promote greater cell division and enlargement, leading to larger-sized oranges compared to those grown in cooler coastal regions. Furthermore, the low relative humidity in stage III (see Figure 9) of citrus production in dry semitropical and subtropical regions, such as in Letsitele and Nelspruit, has been shown to produce citrus with excellent qualities [5, 52]. These qualities include rind color, sugar content, and acidity level. Compared to Nelspruit and Letsitele, the cooler climates of SRV is characterized by lower minimum temperatures (Figure 9). Low temperatures also have depressive effects on fruitlet growth and can result in smaller fruit [53].

Citrusdal and SRV exhibit relatively similar average yearly temperatures and heat units (HU). However, the harvest quality attributes of oranges from Citrusdal are interestingly different from those grown in SRV, and similar to those produced in warmer climates. This may be attributed to variations in temperature, specifically the lower minimum and maximum temperatures observed in Citrusdal, particularly during stage III (Figure 9A-B). Moreover, Citrusdal experiences higher maximum and minimum relative humidity during stage III (Figure 9D) in comparison to SRV. Another contributing factor to the disparity in fruit quality between oranges from SRV and Citrusdal is the difference in vapor pressure deficit (VPD) (Figure 9F). In Citrusdal, there is a pronounced decrease in VPD from stage II to III, which is significantly lower than that of SRV. Lower air temperatures and higher humidity result in reduced VPD, indicating a lower water loss from the fruit rind. This, in turn, facilitates better growth and fruit quality [37], [38]. Therefore, regions with optimal VPD and minimal seasonal variation, particularly during the later stages of fruit growth, as seen in Citrusdal, tend to produce high-quality citrus fruit (refer to supplementary material, Figure S8). These complex interactions between temperature, humidity and VPD can explain the large differences observed between the oranges grown in Citrusdal and SRV. However, the influence of climatic variability in humid climates on rind thickness remains unclear. Nevertheless, citrus exporters should anticipate substantial differences in the quality of citrus fruit harvested from hot semi-arid and humid sub-tropical climates compared to those from Mediterranean and temperate oceanic climates.

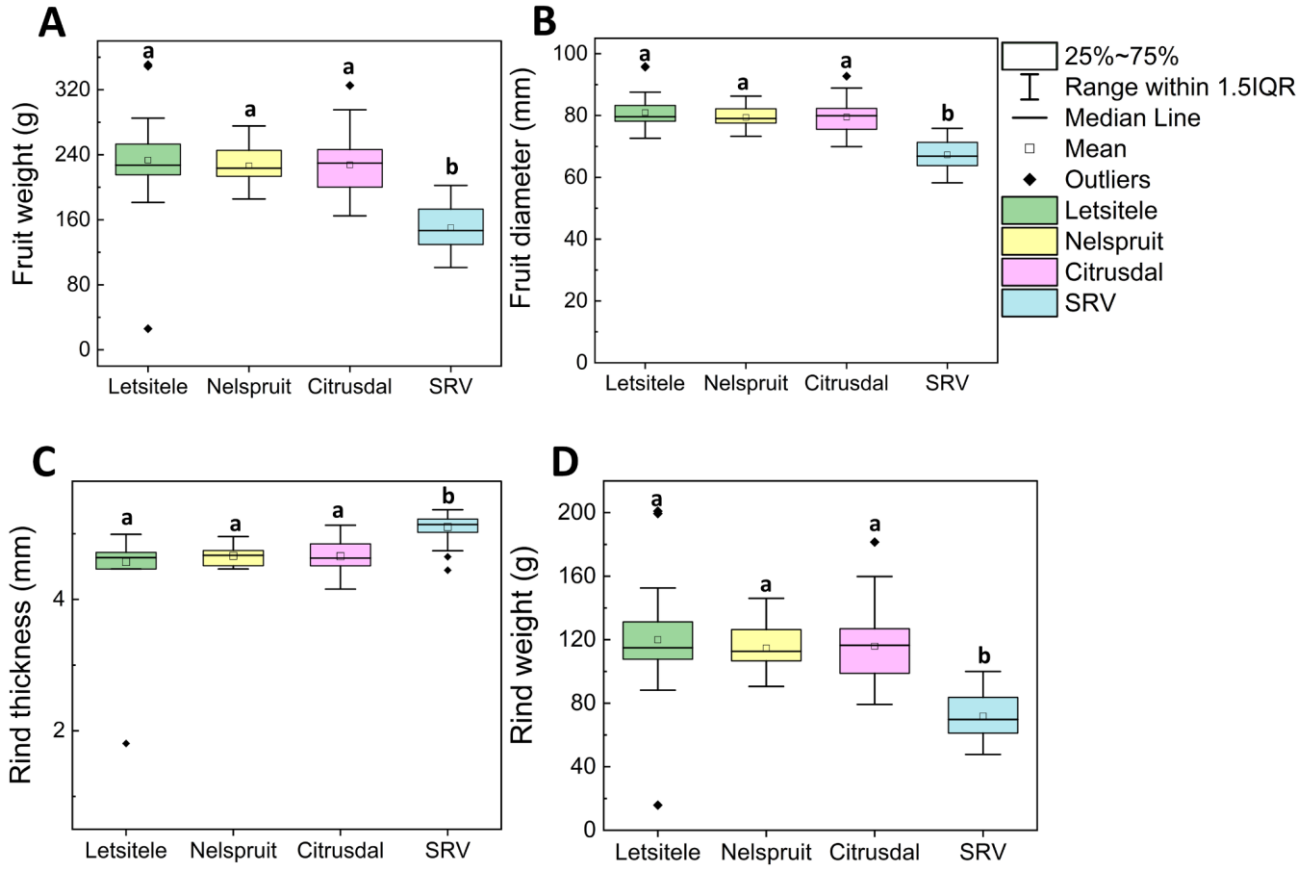

Figure 7. Digital twin output showing the impact of weather variation between growing regions on [A] fruit weight (g), [B] fruit diameter (mm), [C] rind thickness (mm), and [D] rind weight (g) of oranges at harvest. The boxplots represent the median (centre line), 75th upper and 25th lower quartiles (box limits) and 1.5× the interquartile range (IQR, whiskers). Different lower case letters between growing areas, namely, Citrusdal, Letsitele, Nelspruit, and SRV, signify statistically significant at $p \leq 0.05$ (Fisher LSD test, n= 50).

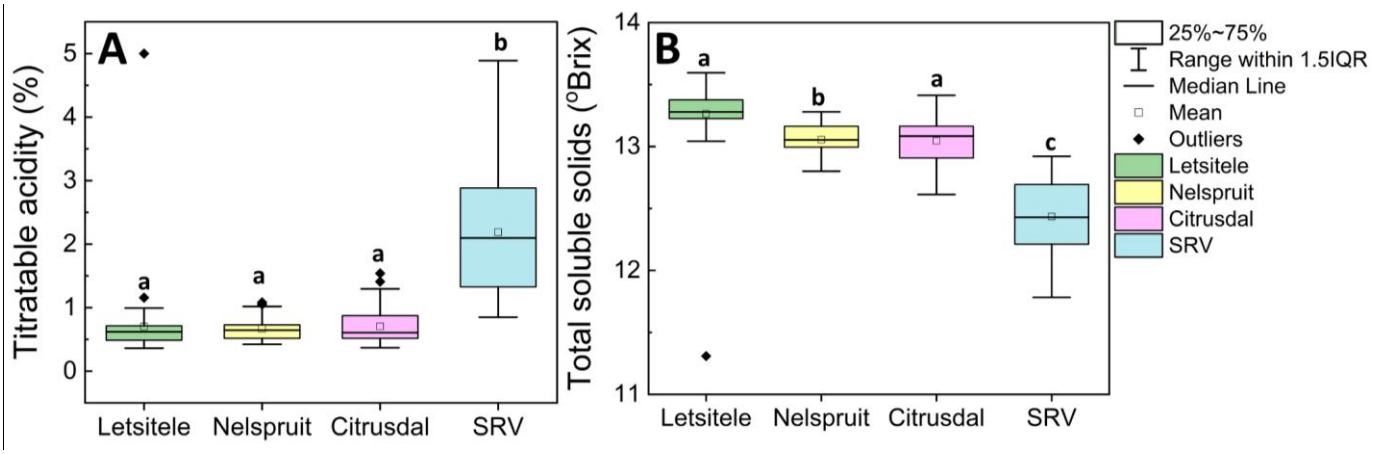

Figure 8. Digital twin output showing the impact of weather variability between growing regions on [A] titratable acidity (%) and [B] total soluble solids (°Brix) of oranges at harvest. The boxplots represent the median (centre line), 75th upper and 25th lower quartiles (box limits) and 1.5× the interquartile range (IQR, whiskers). Different lower case letters between growing areas, namely, Citrusdal, Letsitele, Nelspruit, and SRV, signify statistically significant at $p \leq 0.05$ (Fisher LSD test, n= 50).

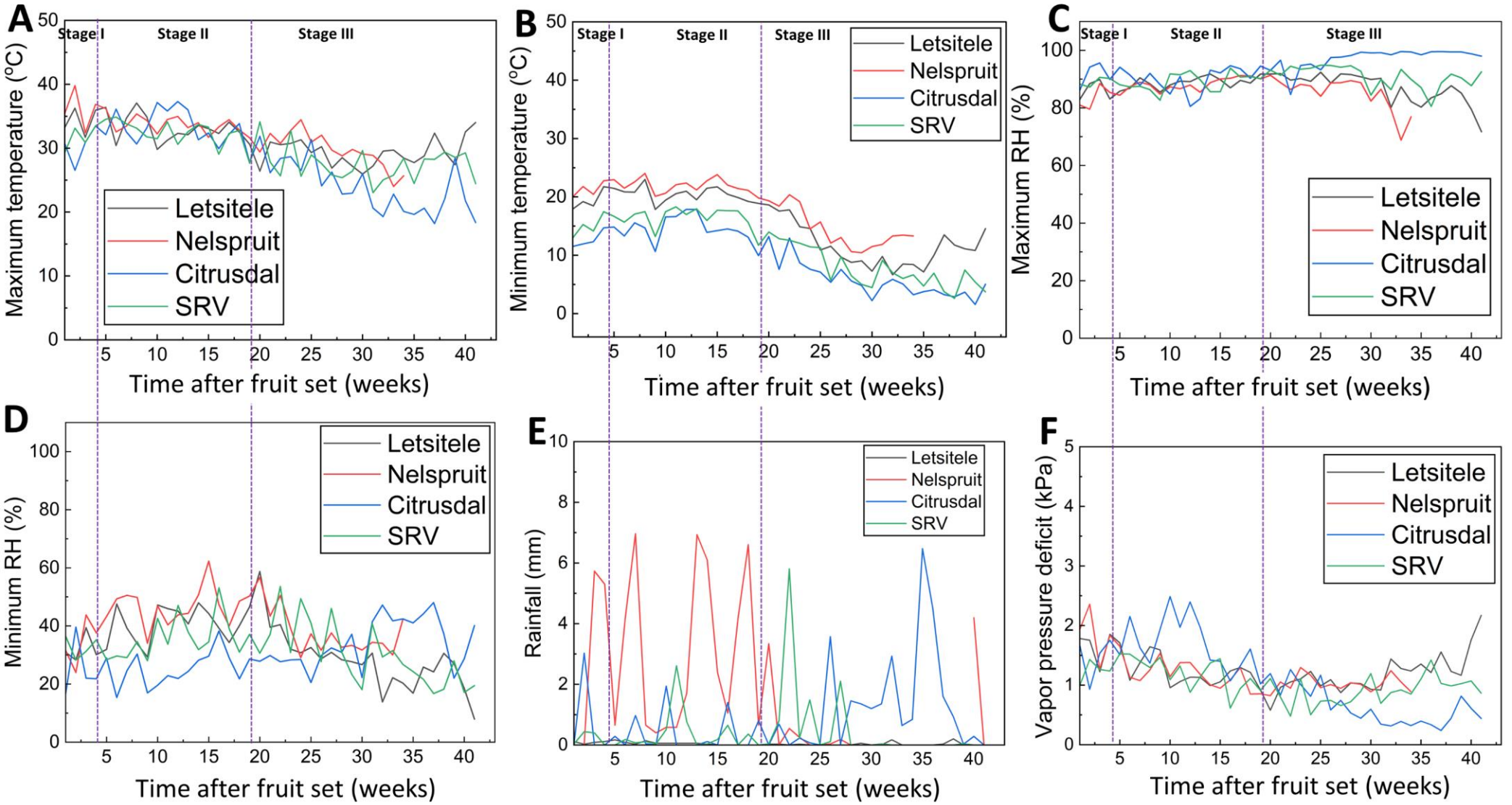

Figure 9. Weekly average [A] maximum temperature (°C), [B] minimum temperature (°C), [C] maximum relative humidity (RH, %), [D] minimum relative humidity (RH, %), [E] rainfall (mm) and [F] vapor pressure deficit (VPD) for 2018/2019 citrus growing season.

3.4 Using digital twins to unveil the spatial-temporal temperature variations of fruit in different growing regions

The digital twin outputs the variations in fruit temperature at both spatial and temporal scales, accounting for changes in physical and thermal parameters during fruit growth and development and between fruit tissues. Figure 10 compares the digital twin output of temperature variability within oranges produced in Letsitele, Nelspruit, Citrusdal, and SRV (using Eqn. 2 - 8; 16 - 21). The daily changes in surface and core fruit temperatures showed similar patterns for all citrus growing regions (Figure 10A). We observe differences between atmospheric air temperature and fruit temperature for all growing regions. Similar to atmospheric air temperature, fruit temperature was highest for oranges produced in the hotter and sunnier climates of Letsitele and Nelspruit compared to the cooler climates of Citrusdal and SRV. The core or center temperature for all growing regions was higher than the fruit surface temperature (Figure 10A). This means that the accumulation of heat generated by the metabolic activities of the fruit and surrounding tissues during growth and development is greater than the effect of convective and radiative heat transfer at the fruit surface. In addition, there is also the cooling effect of evaporation, which significantly reduces the fruit surface temperature.

In most cases, the temperature gradients (difference between core and surface temperature) increased with the time of fruit growth and development for most regions (Figure 10B). This means that the temperature gradients in the fruit at stages II and III were higher than those at stage I. These significant temperature differences within the fruit can even reach up to ~1 °C within a very short time (within 5 weeks after fruit set). The maximum temperature gradients during fruit growth varied across different regions. Letsitele and Citrusdal exhibited a maximum gradient of up to 2.3 °C, Nelspruit had a similar gradient of 2.4 °C, and SRV had the highest maximum gradient of 3.2 °C. The coastal region of SRV had the highest average temperature gradient during plant growth, while the fruit from the warmer climate of Nelspruit displayed the lowest average gradient (Figure 10B). The higher temperature gradients observed in cooler climates than warmer climates can be attributed to the enhanced radiative cooling effect in those regions. Cooler climates generally have lower average temperatures, especially at night, which promotes more significant radiative cooling. Consequently, this temperature differential results in a larger gradient between the core and surface of fruit. Another contributing factor could be the wider diurnal temperature range commonly experienced in cooler climates. During the day, the fruit surface may be exposed to warmer temperatures, elevating the surface temperature (as seen in SRV in Figure 10A). However, during the night, the cooler temperatures impede heat transfer from the fruit core, leading to a larger temperature gradient. Oranges grown in SRV displayed a more pronounced radiative cooling effect compared to Citrusdal, despite Citrusdal having a lower growing temperature (Figure 9A&B). This could be attributed to a greater long-wave radiation cooling effect in SRV compared to Citrusdal (refer to Supplementary material, Figure S9).

This finding is significant because the temperature gradient affect postharvest enzymatic reactions during storage, transport and processing. However, these temperature heterogeneities within the fruit can become even lower in reality due to the small variability in local air movement within different orchards for different growing regions. This effect can be captured by explicitly modeling both free (see section 2.4.3) and forced convection, as well as the fruit's transpiration. As the fruit's surface loses water through transpiration, the air inside the fruit becomes cooler and more humid, thereby reducing core temperature. Note that other factors, such as solar intensity, humidity, canopy

structures and microclimates, and orchard management practices, may, in reality, also contribute to temperature differences within the oranges in these regions.

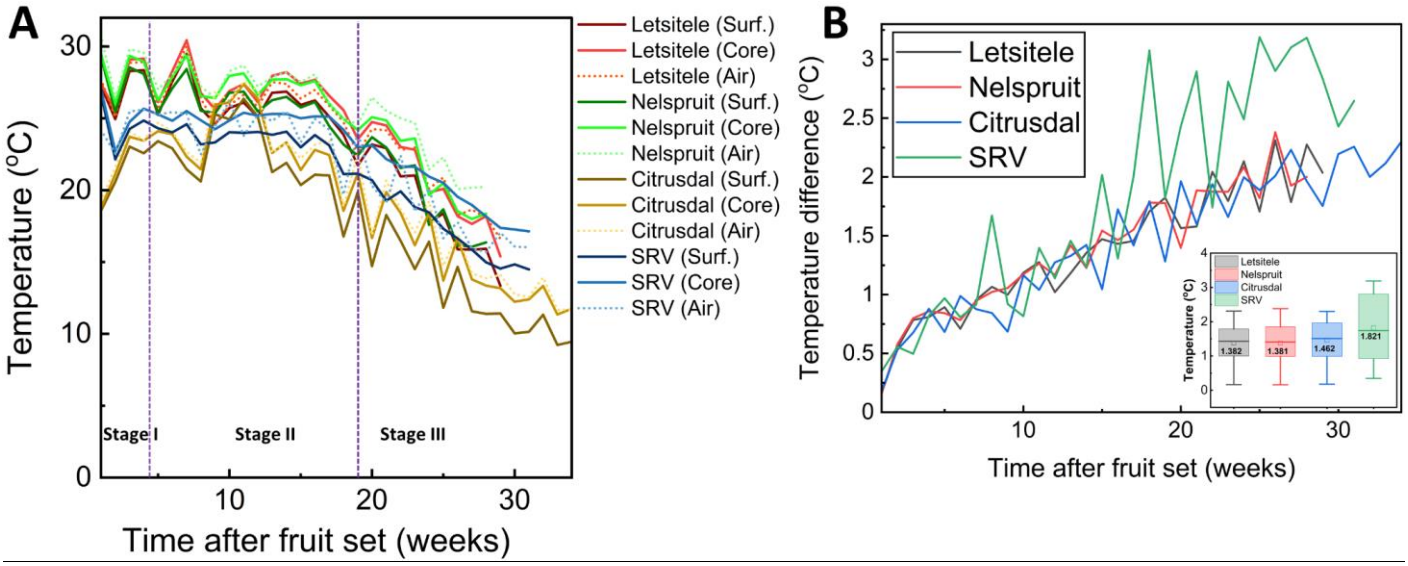

Figure 10. Digital twin output showing [A] Average fruit surface temperature, core temperature and air temperature for Letsitele, Nelspruit, Citrusdal and SRV growing regions as a function of time*; *[B] Temperature difference between the fruit surface and core for Letsitele, Nelspruit, Citrusdal and SRV growing regions as a function of time. The boxplots in [B] represent the mean, median (centre line), 75th upper and 25th lower quartiles (box limits) and 1.5× the interquartile range (IQR, whiskers) of the temperature gradient for different farming regions.

4. LIMITATIONS AND PERSPECTIVE FOR THE CITRUS INDUSTRY

The digital twin of pre-harvest citrus value chains can simulate and predict the impact of variability on the quality evolution of fruit at harvest. The quality parameters at harvest can then serve as an input parameter for a postharvest digital twin from farm to fork. This pioneering study also simulated the impact of a realistic environment (unsteady and non-homogeneous heat fluxes) on the temperature dynamics during the growth of fruit. The final volumetric fruit temperature at harvest serves as an initial condition for the hygrothermal modeling process during postharvest quality evolution of citrus. Current technologies used during citrus production rarely consider measuring fruit temperature during growth. This is because it is challenging to measure directly in the field due to the physical barriers presented by the plant, such as leaves, branches, and other fruit. Obtaining accurate measurements without damaging the fruit or disturbing its growth can be difficult.

With this digital twin concept, stakeholders in the citrus industry can spatially measure and assess how changes in weather, such as temperature, humidity and VPD patterns, could affect citrus postharvest citrus quality. This can help them optimize their operations, improve decision-making, and identify potential risks and opportunities related to climate change. For example, growers can use the digital twin to evaluate the impact of changing climate patterns of a particular growing region on fruit quality. Ultimately, a digital twin of the citrus plant growth process can support more sustainable and resilient citrus production in the face of increasing climatic variability. Nonetheless, this study has some limitations due to the following concerns:

- Weather data from meteorological stations may not accurately represent the microclimate conditions in specific orchards.
- Model calibration data on fruit quality during growth were obtained from literature sources and may differ from actual growth data.
- The EPIC model used in the study did not account for all physiological and structural changes during plant growth, such as tree size and canopy volume, which can vary between warmer and cooler regions.
- The empirical models used for predicting fruit quality evolution may need recalibration for different citrus cultivars.
- Certain model assumptions and factors, such as mass transfer during growth, radiation isotropy, wind direction, fruit shape, and energy exchanges between the plant, flower, and fruit, require further investigation and refinement.

5. CONCLUSIONS

This study quantified the impact of climatic differences between Letsitele, Nelspruit, Citrusdal and Sunday River Valley (SRV) regions of South Africa, on citrus fruit quality at harvest. We did this by developing semi-mechanistic pre-harvest digital twins of 50 Valencia oranges for 10 trees in 5 different orchards per growing region. These digital twins were coupled with measured real-world pre-harvest climate data and predicted fruit quality at harvest. Our study demonstrated that climate variability between growing regions significantly impacts fruit quality at harvest. The key conclusions derived from this study are as follows:

- Our models gave a reasonable prediction for fruit diameter (FD), fruit weight (FW), rind thickness (RT), rind weight (RW), titratable acidity (TA), and total soluble solids (TSS) of oranges at harvest, with an error of less than 20% for Letistele, Nelspruit and SRV.
- The models also accurately captured the impact of weather variability among growing regions on FW, FD, RT, RW, TA and TSS of oranges.
- Due to differences in climatic growing conditions, the fruit diameter (FD), fruit weight (FW), rind thickness (RT), rind weight (RW), titratable acidity (TA) and total soluble solids (TSS) of oranges from different regions are significantly different at harvest. Therefore, stakeholders in the citrus industry should expect statistically significant differences in the harvest quality of citrus grown in hot semi-arid and humid sub-tropical climates with those of Mediterranean and temperate oceanic climates of South Africa.
- Significant differences in fruit temperatures and temperature gradients were found for the different growing regions. The maximal temperature difference within the fruit during the growth and development of oranges produced is up to ~2 °C for those from Letsitele, Nelspruit and Citrusdal, and that of SRV is up to ~3 °C .
- Overall, the growth process of Valencia oranges is complex, involving dynamic changes in FW, FD, RW, RT, TSS, TA and respiration rate that follow a non-linear pattern.

This pioneering study has provided a better understanding of the impact of differences in growing conditions on fruit quality at harvest. Our approach of digital twins of oranges from fruit set to harvest can help growers test the impact of changing cultural practices on fruit quality at harvest. At the same time, this systemic approach can help other citrus supply chain actors to decide when and which growing region would produce quality fruit.

ACKNOWLEDGMENTS

The first author is grateful to Empa for providing the financial resources to conduct this research.

AUTHOR CONTRIBUTIONS

DO: Conceptualization, Literature data collection Methodology, Investigation, Writing Original draft, Review & Editing. **JN:** Experimental data Collection, Review & Editing. **PC:** Experimental data Collection, Review & Editing. **RS:** Review & Editing. **TD:** Conceptualization, Methodology, Review & Editing.

REFERENCES

[1] Ladaniya, M. S. Commercial Fresh Citrus Cultivars and Producing Countries. In *Citrus Fruit: Biology, Technology and Evaluation*; 2008; pp 13–65. https://doi.org/10.1016/B978-0-12-374130-1.50004-8.

[2] Vashisth, T.; Kadyampakeni, D. *Diagnosis and Management of Nutrient Constraints in Citrus*; Elsevier Inc., 2019. https://doi.org/10.1016/B978-0-12-818732-6.00049-6.

[3] Ladaniya, M. S. Introduction. In *Citrus Fruit Biol. Technol. Eval. Citus fruit*; 2008; pp 1–11. https://doi.org/10.1016/B978-0-12-374130-1.50003-6.

[4] Onwude, D. I.; Bahrami, F.; Shrivastava, C.; Berry, T.; Cronje, P.; North, J.; Schudel, S.; Crenna, E.; Shoji, K.; Defraeye, T. Physics-Driven Digital Twins to Quantify the Impact of Pre- and Postharvest Variability on the End Quality Evolution of Orange Fruit. *Resour. Conserv. Recycl.*, **2022**, *186* (February), 1–32. https://doi.org/10.1016/j.resconrec.2022.106585.

[5] Davies, F. S. An Overview of Climatic Effects on Citrus Flowering and Fruit Quality in Various Parts of the World. *Proc. citrus Flower. fruit short course*, **1997**, 1–4.

[6] Lado, J.; Rodrigo, M. J.; Zacarías, L. Maturity Indicators and Citrus Fruit Quality. *Stewart Postharvest Rev.*, **2014**, *10* (2).

[7] Ashebre, K. M. Pre-Harvest and Post-Harvest Factors Affecting Citrus Fruit and Post-Harvest Treatments. *J. Biol. Agric. Healthc.*, **2011**, *5* (23), 19–29.

[8] Ladaniya, M. S. Growth, Maturity, Grade Standards, and Physico-Mechanical Characteristics of Fruit. In *Citrus Fruit: Biology, Technology and Evaluation*; 2008; pp 191–213. https://doi.org/10.1016/B978-0-12-374130-1.50009-7.

[9] Sarkar, T.; Roy, A.; Choudhary, S. M.; Sarkar, S. K. Impact of Climate Change and Adaptation Strategies for Fruit Crops. *Springer Clim.*, **2021**, 79–98. https://doi.org/10.1007/978-3-030-67865-4_4.

[10] Balfagón, D.; Arbona, V.; Gómez-Cadenas, A. THE FUTURE OF CITRUS FRUIT: The Impact of Climate Change on Citriculture. *Metode*, **2022**, *2022* (12), 123–129. https://doi.org/10.7203/metode.12.20319.

[11] Ali, M. M.; Yousef, A. F.; Li, B.; Chen, F. Effect of Environmental Factors on Growth and Development of Fruits. *Trop. Plant Biol.*, **2021**, *14* (3), 226–238. https://doi.org/10.1007/s12042-021-09291-6.

[12] K, M.; Leffelaar, P. A.; Kropff, M. J. On Approaches and Applications of the Wageningen Crop Models. *Eur. J. Agron.*, **2003**, *18*.

[13] BAI, T. cheng; WANG, T.; ZHANG, N. nan; CHEN, Y. qi; MERCATORIS, B. Growth Simulation and Yield Prediction for Perennial Jujube Fruit Tree by Integrating Age into the WOFOST Model. *J. Integr. Agric.*, **2020**, *19* (3), 721–734. https://doi.org/10.1016/S2095-3119(19)62753-X.

[14] Zhao, C.; Liu, B.; Xiao, L.; Hoogenboom, G.; Boote, K. J.; Kassie, B. T.; Pavan, W.; Shelia, V.; Kim, K. S.; Hernandez-Ochoa, I. M.; et al. A SIMPLE Crop Model. *Eur. J. Agron.*, **2019**, *104* (February), 97–106. https://doi.org/10.1016/j.eja.2019.01.009.

[15] Tijskens, L. M. M.; Unuk, T.; Okello, R. C. O.; Wubs, A. M.; Šuštar, V.; Šumak, D.; Schouten, R. E. From Fruitlet to Harvest: Modelling and Predicting Size and Its Distributions for Tomato, Apple and Pepper Fruit. *Sci. Hortic. (Amsterdam).*, **2016**, *204*, 54–64. https://doi.org/10.1016/j.scienta.2016.03.036.

[16] Ribeiro, T. D.; De Mattos, R. W. P.; De Morais, A. R.; Muniz, J. A. Description of the Growth of Pequi Fruits by Nonlinear Models. *Rev. Bras. Frutic.*, **2018**, *40* (4), 1–11. https://doi.org/10.1590/0100-29452018949.

[17] Yang, H.; Du, T.; Mao, X.; Ding, R.; Shukla, M. K. A Comprehensive Method of Evaluating the Impact of Drought and Salt Stress on Tomato Growth and Fruit Quality Based on EPIC Growth Model. *Agric. Water Manag.*, **2019**, *213* (October 2018), 116–127. https://doi.org/10.1016/j.agwat.2018.10.010.

[18] Nawaz, R.; Abbasi, N. A.; Hafiz, I. A.; Khalid, A. Impact of Climate Variables on Growth and Development of Kinnow Fruit (Citrus Nobilis Lour x Citrus Deliciosa Tenora) Grown at Different Ecological Zones under Climate Change Scenario. *Sci. Hortic. (Amsterdam).*, **2020**, *260* (October 2019). https://doi.org/10.1016/j.scienta.2019.108868.

[19] Defraeye, T.; Shrivastava, C.; Berry, T.; Verboven, P.; Onwude, D.; Schudel, S.; Bühlmann, A.; Cronje, P.; Rossi, R. M. Digital Twins Are Coming: Will We Need Them in Supply Chains of Fresh Horticultural Produce? *Trends Food Sci. Technol.*, **2021**, *109* (March 2020), 245–258. https://doi.org/10.1016/j.tifs.2021.01.025.

[20] Alexander, M. South Africa's weather and climate https://southafrica-info.com/.

[21] Citrus Academy. Citrus Planting Management Learner Guide. *2 Citrus Types Cultiv.*, **2017**, *3650* (031), 14.

[22] Koverda, P. The Ultimate Vapor Pressure Deficit (VPD) Guide https://pulsegrow.com/blogs/learn/vpd.

[23] Hardy, S.; Khurshid, T. *Calculating Heat Units for Citrus*; 2021.

[24] Bain, J. Morphological , Anatomical, and Physiological Changes in the Developing Fruit of the Valencia Orange , Citrus Sinensis (L .) Osbeck. *Aust. J. Bot.*, **1957**, *6* (1), 1–23.

[25] Abu-Goukh, A.-B.; Shattir, A.; Mahdi, E. F. Physico-Chemical Changes during Growth and Development of Papaya Fruit. II: Chemical Changes. *Agric. Biol. J. North Am.*, **2010**, *1* (5), 871–877. https://doi.org/10.5251/abjna.2010.1.5.871.877.

[26] Jame, Y. W.; Cutforth, H. W. Crop Growth Models for Decision Support Systems. *Can. J. Plant Sci.*, **1996**, *76* (1), 9–19. https://doi.org/10.4141/cjps96-003.

[27] Williams, J. R.; Jones, C. A.; Kiniry, J. R.; Spanel, D. A. EPIC Crop Growth Model. *Trans. Am. Soc. Agric. Eng.*, **1989**, *32* (2), 497–511.

[28] Choruma, D.; Balkovic, J.; Odume, O. N. Calibration and Validation of the EPIC Model for Maize Production in the Eastern Cape, South Africa. *Agronomy*, **2019**, *9* (9), 1–16. https://doi.org/10.3390/agronomy9090494.

[29] Roy, P. P.; Paul, S.; Mitra, I.; Roy, K. On Two Novel Parameters for Validation of Predictive QSAR Models. *Molecules*, **2009**, *14* (5), 1660–1701. https://doi.org/10.3390/molecules14051660.

[30] Roy, P. P.; Roy, K. On Some Aspects of Variable Selection for Partial Least Squares Regression Models. *QSAR Comb. Sci.*, **2008**, *27* (3), 302–313. https://doi.org/10.1002/qsar.200710043.

[31] Turrell, F. M.; Garber, M. J.; Jones, W. W.; Cooper, W. C.; Young, R. H. Growth Equations and Curves for Citrus Trees. *Hilgardia*, **1969**, *39* (16), 429–445. https://doi.org/10.3733/hilg.v39n16p429.

[32] Sasikumar, R.; Vivek, K.; Chakkaravarthi, S.; Deka, S. C. Physicochemical Characterization and Mass Modeling of Blood Fruit (Haematocarpus Validus)–An Underutilized Fruit of Northeastern India. *Int. J. Fruit Sci.*, **2021**, *21* (1), 12–25. https://doi.org/10.1080/15538362.2020.1848752.

[33] Reuther, W.; Rasmussen, G. K.; Hilgeman, R. H.; Cahoon, G. A.; Cooper, W. C. A Comparison of Maturation and Composition of 'Valencia' Oranges in Some Major Subtropical Zones of the United States1. *J. Am. Soc. Hortic. Sci.*, **1969**, *94* (2), 144–157. https://doi.org/10.21273/jashs.94.2.144.

[34] Ladaniya, M. S.; Mahalle, B. C. Fruit Maturation and Associated Changes in "Mosambi" Orange (Citrus Sinensis). *Indian J. Agric. Sci.*, **2011**, *81* (6), 494–499.

[35] Parra-Coronado, A.; Fischer, G.; Camacho-Tamayo, J. H. Model of Pre-Harvest Quality of Pineapple Guava Fruits (Acca Sellowiana (O. Berg) Burret) as a Function of Weather Conditions of the Crops. *Bragantia*, **2017**, *76* (1), 177–186. https://doi.org/10.1590/1678-4499.652.

[36] Colauto Stenzel, N. M.; Janeiro Neves, C. S. V.; Marur, C. J.; Dos Santos Scholz, M. B.; Gomes, J. C. Maturation Curves and Degree-Days Accumulation for Fruits of "folha Murcha" Orange Trees. *Sci. Agric.*, **2006**, *63* (3), 219–225. https://doi.org/10.1590/S0103-90162006000300002.

[37] Abu-Goukh, A.-B.; Shattir, A.; Mahdi, E. F. Physico-Chemical Changes during Growth and Development of Grapefruits Fruit. II: Chemical Changes. *Agric. Biol. J. North Am.*, **2010**, *1* (5), 871–877. https://doi.org/10.5251/abjna.2010.1.5.871.877.

[38] Saudreau, M.; Marquier, A.; Adam, B.; Sinoquet, H. Modelling Fruit-Temperature Dynamics within Apple Tree Crowns Using Virtual Plants. *Ann. Bot.*, **2011**, *108* (6), 1111–1120. https://doi.org/10.1093/aob/mcr054.

[39] Saudreau, M.; Sinoquet, H.; Santin, O.; Marquier, A.; Adam, B.; Longuenesse, J. J.; Guilioni, L.; Chelle, M. A 3D Model for Simulating the Spatial and Temporal Distribution of Temperature within Ellipsoidal Fruit. *Agric. For. Meteorol.*, **2007**, *147* (1–2), 1–15. https://doi.org/10.1016/j.agrformet.2007.06.006.

[40] Cengel, Y. A.; Ghajar, A. J. *Heat and Mass Transfer: Fundamentals and Applications*; McGraw-Hill Education: 2 Penn Plaza, New York, 2011.

[41] Whitaker, S. Forced Convection Heat Transfer Correlations for Flow in Pipes, Past Flat Plates, Single Cylinders, Single Spheres, and for Flow in Packed Beds and Tube Bundles. *AIChE J.*, **1972**, *18* (2), 361–371. https://doi.org/10.1002/aic.690180219.

[42] Michaletz, S. T.; Johnson, E. A. Foliage Influences Forced Convection Heat Transfer in Conifer Branches and Buds. *New Phytol.*, **2006**, *170* (1), 87–98. https://doi.org/10.1111/j.1469-8137.2006.01661.x.

[43] Becker, B. R.; Misra, A.; Fricke, B. A. Bulk Refrigeration of Fruits and Vegetables Part I: Theoretical Considerations of Heat and Mass Transfer. *HVAC R Res.*, **1996**, *2* (2), 122–134. https://doi.org/10.1080/10789669.1996.10391338.

[44] ASHRAE. *Ashrae Handbook- Refrigeration: Systems and Applications*; Atlanta, 2018.

[45] Sharpe, P. J. H.; Barber, H. N. Near Infrared Reflectance of Colored Fruits. *Appl. Opt.*, **1972**, *11* (12), 2902. https://doi.org/10.1364/ao.11.002902.

[46] Gaffney, J. J. Reflectance Properties of Citrus Fruits. *Trans. ASABE*, **1973**, 310–314.

[47] Caselles, V.; Sobrino, J. A.; Becker, F. Determination of the Effective Emissivity and Temperature under Vertical Observation of a Citrus Orchard. Application to Frost Nowcasting. *Int. J. Remote Sens.*, **1988**, *9* (4), 715–727. https://doi.org/10.1080/01431168808954888.

[48] Onwude, D. I.; Hashim, N.; Abdan, K.; Janius, R.; Chen, G.; Kumar, C. Modelling of Coupled Heat and Mass Transfer for Combined Infrared and Hot-Air Drying of Sweet Potato. *J. Food Eng.*, **2018**, *228*, 12–24. https://doi.org/10.1016/j.jfoodeng.2018.02.006.

[49] Telis-Romero, J.; Telis, V. R. N.; Gabas, A. L.; Yamashita, F. Thermophysical Properties of Brazilian Orange Juice as Affected by Temperature and Water Content. *J. Food Eng.*, **1998**, *38* (1–4), 27–40. https://doi.org/10.1016/s0260-8774(98)00107-1.

[50] SWEAT, V. E. Experimental Values of Thermal Conductivity of Selected Fruits and Vegetables. *J. Food Sci.*, **1974**, *39* (6), 1080–1083. https://doi.org/10.1111/j.1365-2621.1974.tb07323.x.

[51] Jorgensen, S. E. Fundamentals of Ecological Modelling. *Oceanogr. Lit. Rev.*, **1995**, *9* (42), 759–760.

[52] Goldschmidt, E. E. Effect of Climate on Fruit Development and Maturation. *Citrus Flower. Fruiting Short Course. Citrus Res. Educ. Cent.*, **1997**, 93–97.

[53] Agustí, M.; Primo-Millo, E. *Flowering and Fruit Set*; Elsevier Inc., 2020. https://doi.org/10.1016/B978-0-12-812163-4.00011-5.

[54] Grossiord, C.; Buckley, T. N.; Cernusak, L. A.; Novick, K. A.; Poulter, B.; Siegwolf, R. T. W.; Sperry, J. S.; McDowell, N. G. Plant Responses to Rising Vapor Pressure Deficit. *New Phytol.*, **2020**, *226* (6), 1550–1566. https://doi.org/10.1111/nph.16485.

[55] Massmann, A.; Gentine, P.; Lin, C. When Does Vapor Pressure Deficit Drive or Reduce Evapotranspiration? *J. Adv. Model. Earth Syst.*, **2019**, *11* (10), 3305–3320. https://doi.org/10.1029/2019MS001790.

SUPPLEMENTARY MATERIAL

1. Production region and fruit sampling

Five commercial orchards within each production region of Letsitele, Nelspruit, Citrusdal and SRV were selected for Valencia orange cultivar, as presented in Table S1. Standard commercial management practices to produce export-quality fruit were employed in all experimental orchards. The experimental layout was a completely randomized design, where the production region was the treatment, whilst the orchards within a production region provided statistical replication (n=5). Within each orchard, ten healthy adjacent trees, uniform in size and vigor, were selected, tagged, and reserved for sampling throughout the three production seasons. Fruit was harvested at commercial maturity, as determined for a cultivar by producers in a region, thus resulting in different harvesting times, with the northern being earlier than the southern regions. Fifteen fruit per tree were sampled from the outside up to 30 cm within the canopy to obtain 150 fruit per orchard and pooled as a replicate to use for subsequent measurements. Fruit of similar diameter, color and free from rind defects, were selected to reduce sample variation.

Table S1. Production information on experimental sites and the cultivars used to evaluate production region and climactic differences as possible factors that may affect the susceptibility of fruit to CI.

Production region	Cultivar	Orchard number	Rootstock	Year planted	Planting density (m)
Letsitele	Turkey	Orchard 1	SC	2003	7 x 3
Letsitele	Turkey	Orchard 2	SC	2003	7 x 3
Letsitele	Turkey	Orchard 3	SC	2002	7 x 3
Letsitele	Turkey	Orchard 4	SC	2001	7 x 3
Letsitele	Turkey	Orchard 5	CC	2004	7 x 3
Nelspruit	Turkey	Orchard 1	CC/C35	2003	6 × 2.5
Nelspruit	Turkey	Orchard 2	CC/C35	2003	6 × 2.5
Nelspruit	Turkey	Orchard 3	CC/C35	2003	6 × 2.5
Nelspruit	Turkey	Orchard 4	SC/X639	2000	5 x 2.5
Nelspruit	Turkey	Orchard 5	SC/X639	2000	5 x 2.5
Citrusdal	Turkey	Orchard 1	RL	1995	7 x 4
Citrusdal	Turkey	Orchard 2	RL	1995	7 x 4
Citrusdal	Turkey	Orchard 3	CC	1996	5 x 2
Citrusdal	Turkey	Orchard 4	CC	1996	5 x 2
Citrusdal	Turkey	Orchard 5	CC	2008	5 x 2
SRV	Turkey	Orchard 1	CC	2005	6 x 3

SRV	Turkey	Orchard 2	CC	2003	6 x 2.5
SRV	Turkey	Orchard 3	SC	2007	6 x 2.5
SRV	Turkey	Orchard 4	CC	2005	6 x 2
SRV	Turkey	Orchard 5	CC	2001	5 x 2

2. Model calibration

Fruit growth model

In Figure S1, we compared the predicted fruit size data with the corresponding experimental data from the literature [1]. The experimental data were collected from Valencia oranges provided by the late Nr. G. Linton from Somersby via Gosford, N.S.W. The oranges were harvested from 30-year old trees that received five 2-lb dressings of ammonium sulphate throughout the year. Full blossom for the 1954 season occurred on November 17, 1953, which was about a month later than the usual date. Commercial picking took place in December 1954, which was approximately 56 weeks after blossom. The final experimental pick was made on January 4, 1955, which was 59 weeks after full blossom. The figure shows that the predicted fruit size data agree reasonably well with the experimental data of Valencia orange with $R^2 = 0.99$.

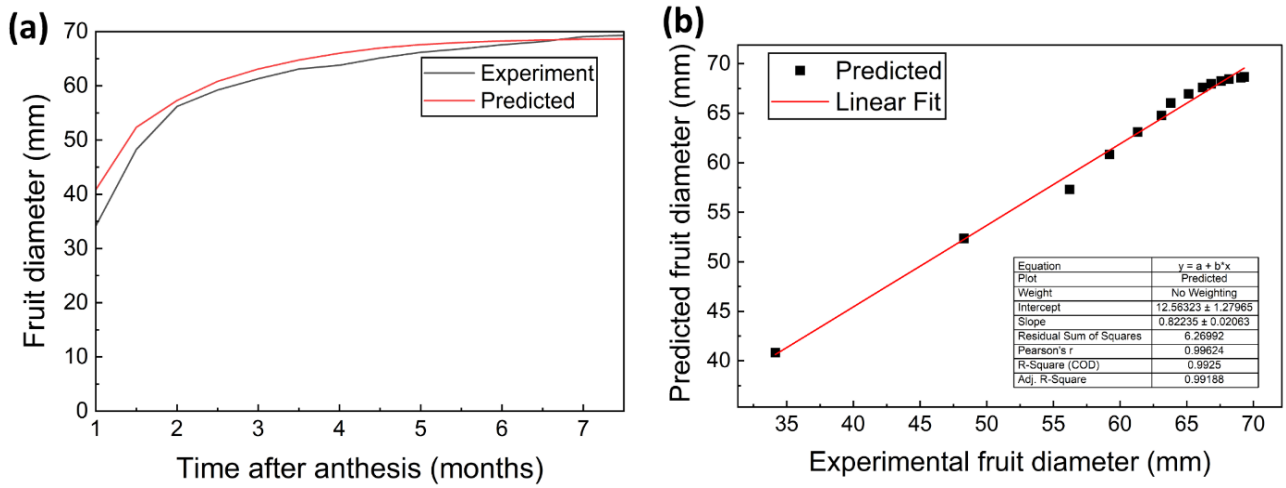

Figure S1. (a) Average experimental and simulated fruit growth profile of Valencia orange; (b) Calibration plot of predicted fruit diameter data and that of experimental data [1]. Note that the simulated data is based on the Letsitele production region.

Calibration plot for fruit diameter (FD)

The exponential function gave a reasonable prediction of fruit diameter (FD, mm) based on the measured fruit weight (FW, g). The model was calibrated using growth data of 1067 Valencia oranges from two growing seasons in Gosford district of New South Wales [1]. The calibration plot is shown in Figure S2.

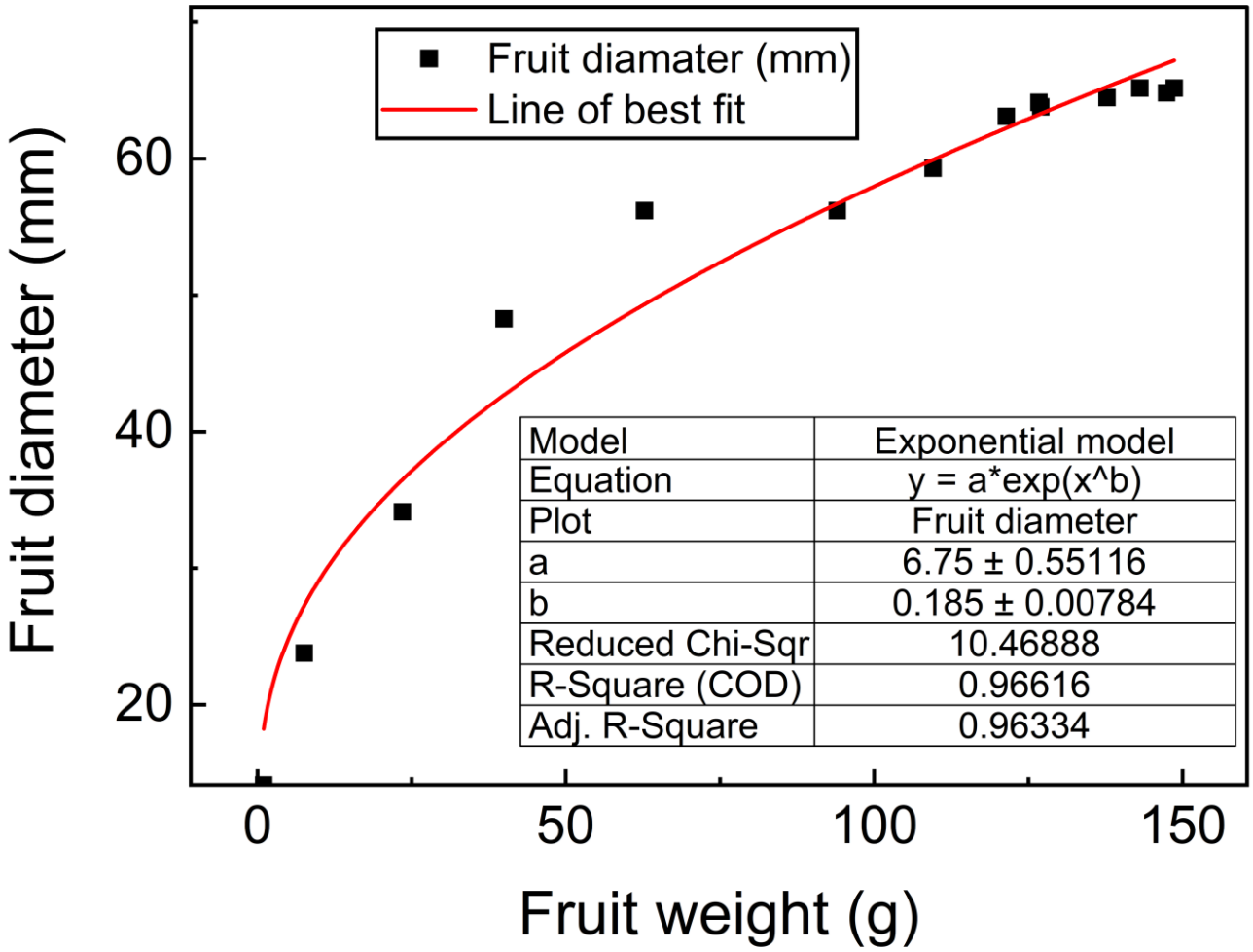

Figure S2. Calibration plot for fruit diameter (mm) based on fruit weight (g) for Valencia orange.

Calibration plot for rind weight (RW)

The exponential function also gave a reasonable prediction of rind weight (RW, g) based on the measured fruit weight (FW, g). The model was calibrated using growth data of 1067 Valencia oranges from two growing seasons in Gosford district of New South Wales [1]. The calibration plot is shown in Figure S3.

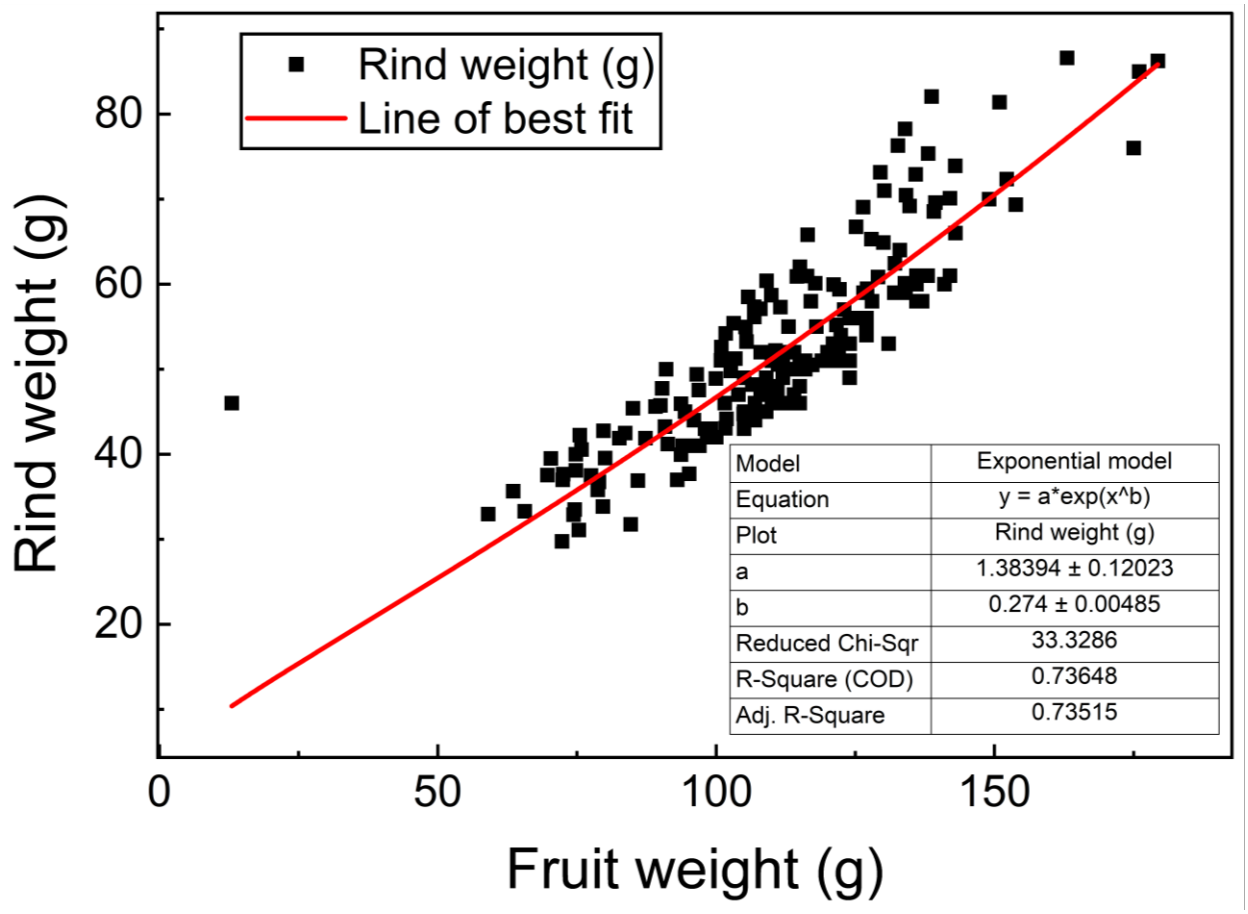

Figure S3. Calibration plot for rind weight (g) based on fruit weight (g) for Valencia orange.

Calibration plot for rind thickness (RT)

The use of a piecewise function yielded an accurate prediction of rind thickness (RT, mm) based on fruit diameter (FD, mm) and calibrated using data from [2]. The results of the calibration are presented in Figure S4.

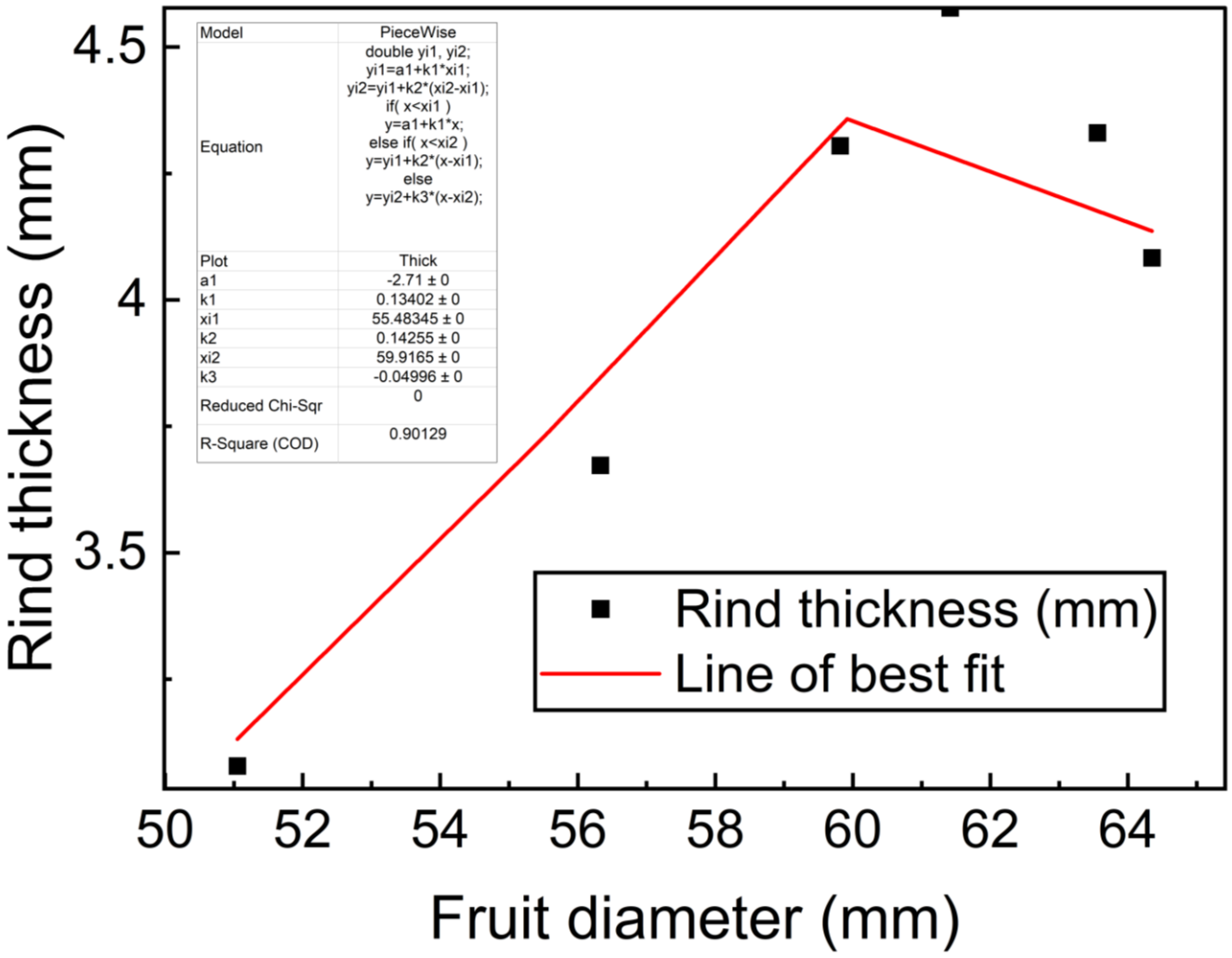

Figure S4. Calibration plot for rind thickness (mm) based on fruit diameter (mm) for Valencia orange.

Calibration plot for heat of respiration (RP)

The heat of respiration (RP, W/kg) during plant growth and development was obtained from an exponential decay relationship with fruit weight (FW, kg) and calibrated with same experimental data as previous parameters from [1]. The calibration plot is shown in Figure S5.

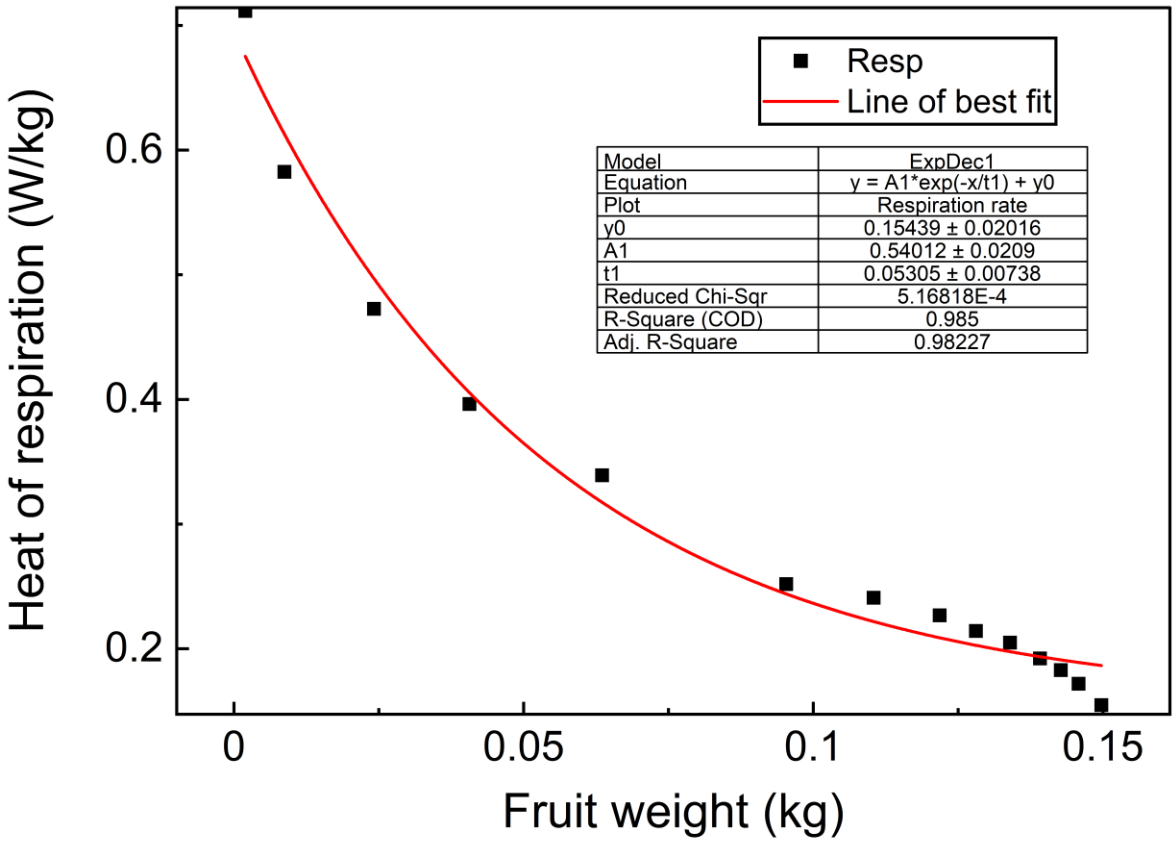

Figure S5. Calibration plot for heat of respiration during plant growth and development (W/kg) based on fruit weight (kg) for Valencia orange.

Calibration plot for total soluble solids (TSS)

The total soluble solids (TSS, °Brix) during plant growth and development was obtained from a polynomial relationship with respiration rate (RP, mgCO_2/kg/hr) and calibrated with experimental data from [3]. The calibration plot is shown in Figure S6.

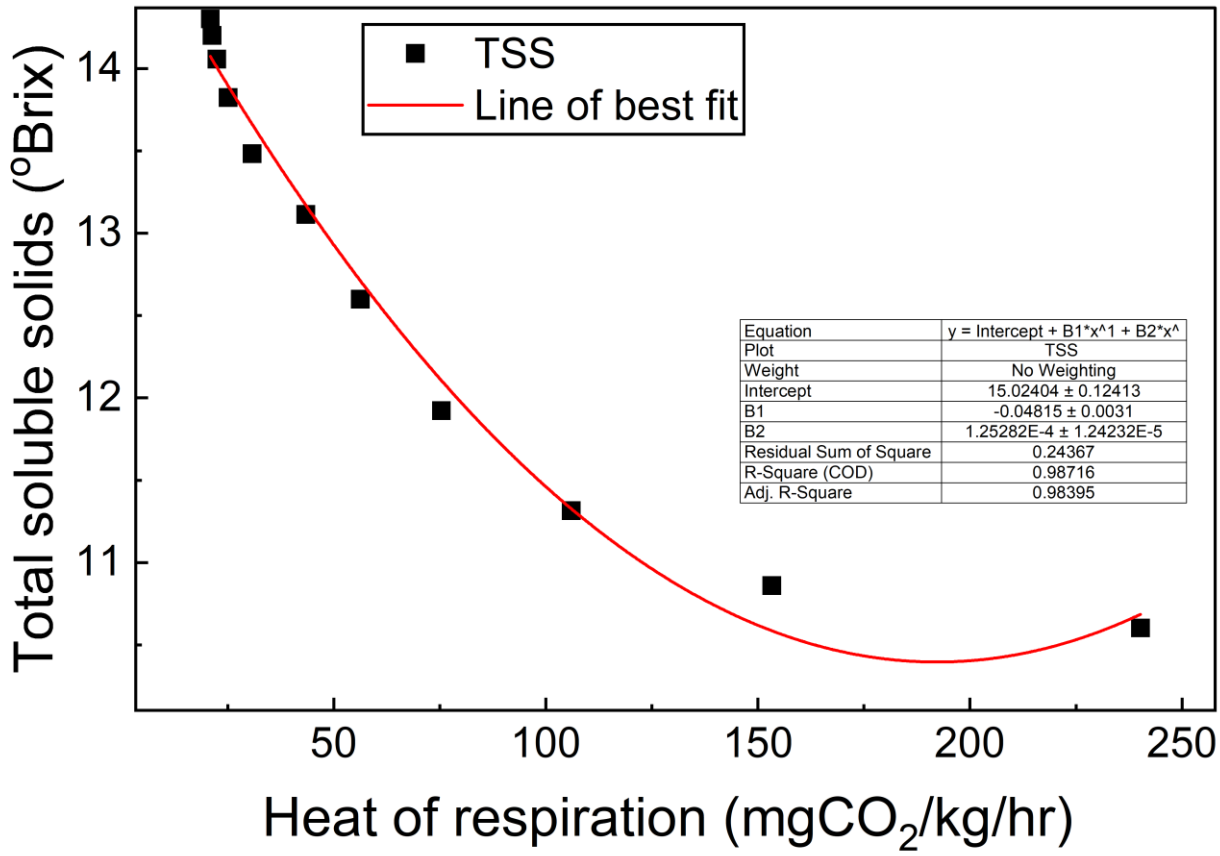

Figure S6. Calibration plot for total soluble solids (°Brix) based on heat of respiration (mgCO₂/kg/hr) for citrus.

Calibration plot for titratable acidity (TA)

The titratable acidity (TA, %) during plant growth and development was obtained from a polynomial relationship with respiration rate (RP, mgCO₂/kg/hr) and calibrated with experimental data from [3]. The calibration plot is shown in Figure S6.

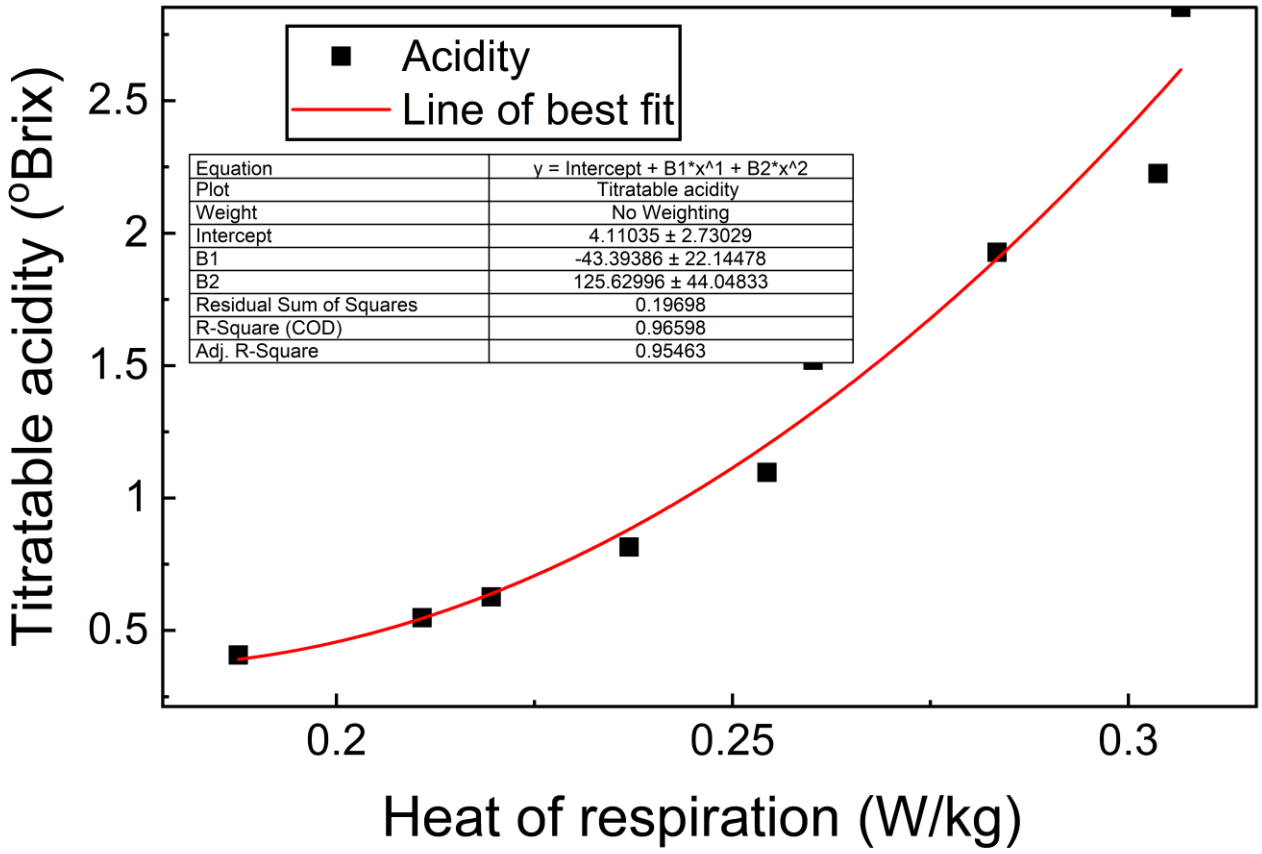

Figure S7. Calibration plot for titratable acidity (%) based on heat of respiration (mgCO₂/kg/hr) for citrus.

3. Impact of weather variation between growing regions on fruit quality attributes at harvest

We assess the influence of seasonal variability of growing conditions on fruit quality properties of oranges at harvest for Citrusdal and Sunday River's Valley (SRV). To do this, we conducted a correlation analysis between seasonal variability of maximum temperature (Tx), minimum temperature (Tn), maximum relative humidity (RHx), minimum relative humidity (RHn), and vapor pressure deficit (VPD), with the fruit quality parameters of fruit diameter (FD), titratable acidity (TA), and total soluble solids (TSS) in the Citrusdal and Sunday River's Valley (SRV) regions during the 2018/2019 and 2019/2020 citrus growing seasons (Figure S8). Data were obtained using the Agricultural Research Council (ARC) automated weather stations (see section 2.2.3 in the main manuscript). Figure S8A presents the Pearson's correlation coefficients between the standard deviation of Tx, Tn, RHx RHn, and VPD (x-axis in red) and the fruit quality parameters of FD, TA, and TSS (y-axis in green) for Citrusdal. The analysis reveals that in the Citrusdal region, there is a significant correlation between the standard deviation of RHx and VPD and the fruit quality parameters of FD, TA, and TSS. This suggests that seasonal variations in RHx and VPD contribute to variations in FD, TA, and TSS in the Citrusdal region. However, in the SRV region, there is no significant correlation between the standard deviation of the growing conditions (including RHx and VPD) and the fruit quality parameters of FD, TA, and TSS (Figure S8B). This indicates that seasonal variations in the growing conditions do not significantly impact the FD,

TA, and TSS variation in the SRV region. These findings highlight the region-specific relationship between the standard deviation of RHx and VPD and the fruit quality parameters in citrus production. Understanding these correlations can provide valuable insights for optimizing growing conditions and enhancing fruit quality in the Citrusdal region.

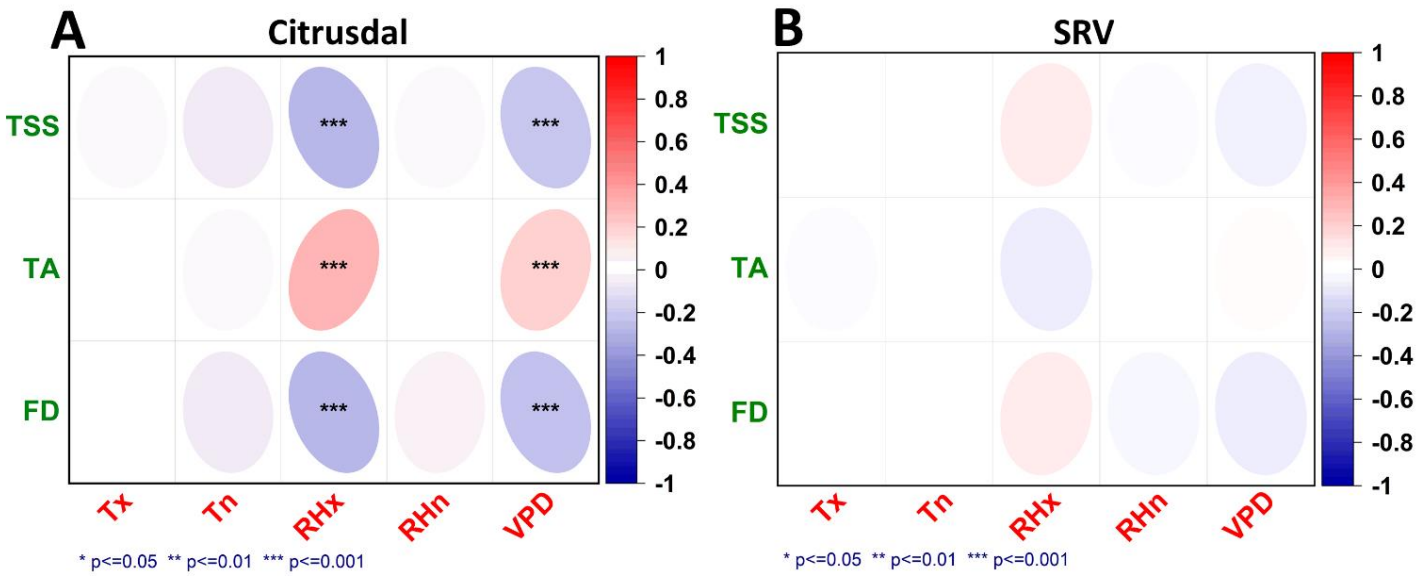

Figure S8. Pearson's correlation coefficients of the standard deviation of maximum temperature (Tx, °C), minimum temperature (Tn, °C), maximum relative humidity (RHx, %), minimum relative humidity (RHn, %), and vapor pressure deficit (VPD) (x-axis in red) on fruit diameter (FD, mm), titratable acidity (TA, %, and total soluble solids (TSS, °Brix) of oranges (y-axis in green), for [A] Citrusdal, and [B] Sunday River's Valley (SRV) regions during the for 2018/2019 and 2019/2020 citrus growing seasons. The positive (red) and negative (blue) correlation are indicated, and the color gradient depicts each correlation's strength. Black asterisks represent p-value as *** for p <= 0.001, ** for p <= 0.01, and * for p <= 0.05.

4. Radiative cooling effect

Despite Citrusdal having a lower temperature compared to SRV during the 2018/2019 season (refer to Figure 9 in the main manuscript), oranges grown in SRV exhibited a more noticeable radiative cooling effect than those in Citrusdal. This difference can be attributed to a greater long-wave radiation cooling effect in SRV as opposed to Citrusdal (see Figure S9). The figure clearly demonstrates that the long-wave radiation in SRV, from stage I to mid-Stage III, is significantly higher than in Citrusdal, with a maximum difference of approximately 49 W m^{-2} in week 16. These substantial variations in long-wave radiation lead to significant differences in the cooling effect, ultimately affecting the fruit temperature and growth dynamics of oranges in different regions.

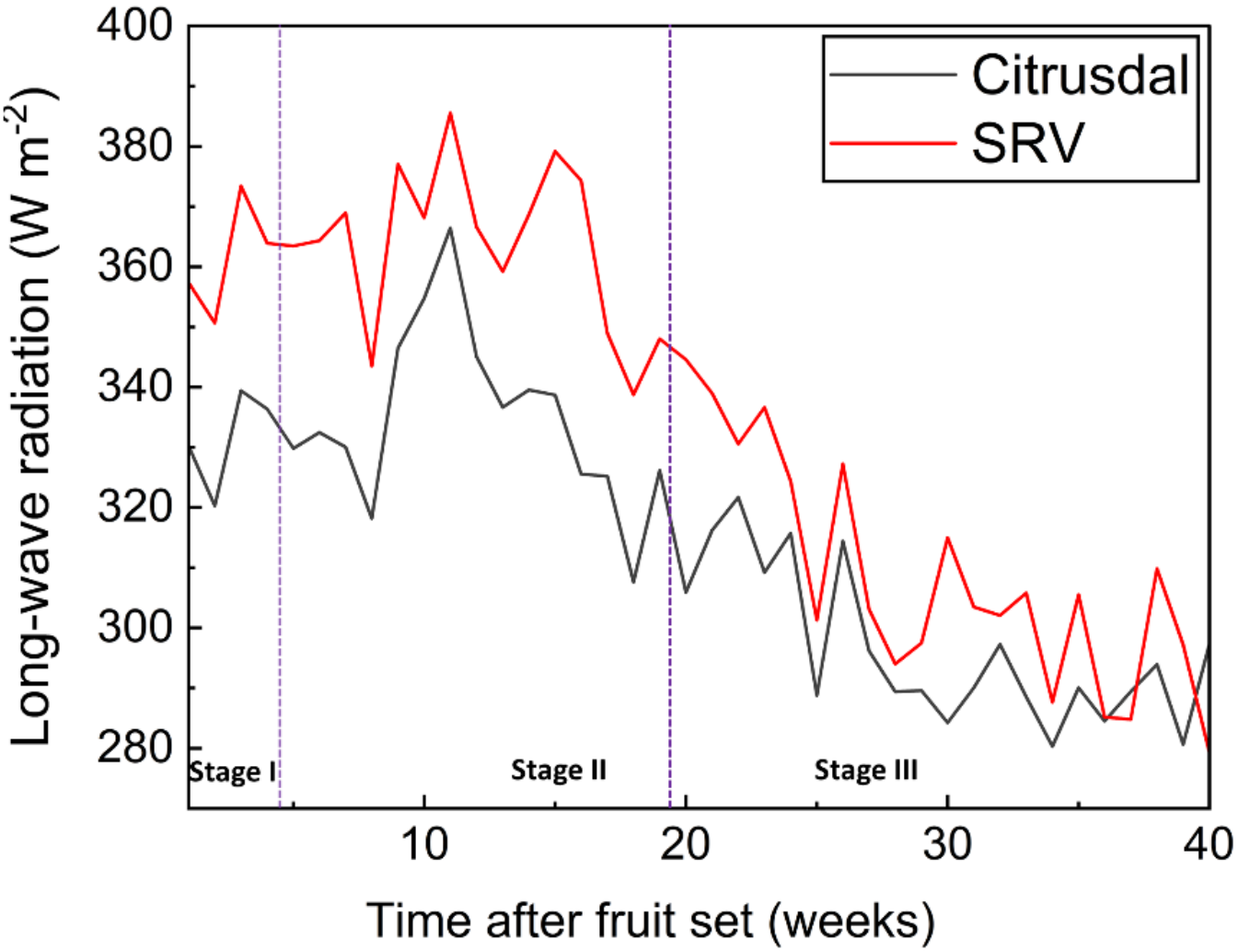

Figure S9. Long-wave radiation of oranges grown in Citrusdal and SRV during the 2018/2019 growing season in South Africa.

5. Grid sensitivity analysis

Based on a grid sensitivity analysis, an appropriate grid was selected for the two-dimensional axisymmetric geometry of orange fruit. As the underlying physics for all growing regions are the same, we determine the optimal mesh settings for Citrusdal and use the same mesh settings for all other regions. We evaluated five different grids: extreme-fine, extra fine (base), fine, coarse and extremely-coarse grids with 11660, 3030, 416, 140, and 16 finite elements, respectively (Figure S10). The finest grid was the extreme-fine grid. A gradual refinement toward the air–rind and pulp interfaces was applied to enhance numerical accuracy and stability, as the largest gradients occur there. Our finding shows that the difference between the finest mesh (extreme-fine) and the most coarse mesh (extremely coarse) for both the fruit surface (Figure 10A) and fruit core (Figure 10B) is less than 0.000029 °C and 0.0002 °C, respectively. This means that all mesh investigated would yield the same result for the physics implemented in this study. We selected the extreme-fine grid as the base in this study to optimize computational load and accuracy. This grid consisted of triangular and quadrilateral finite elements, with a total element size of 3030 and an average element quality of 0.90.

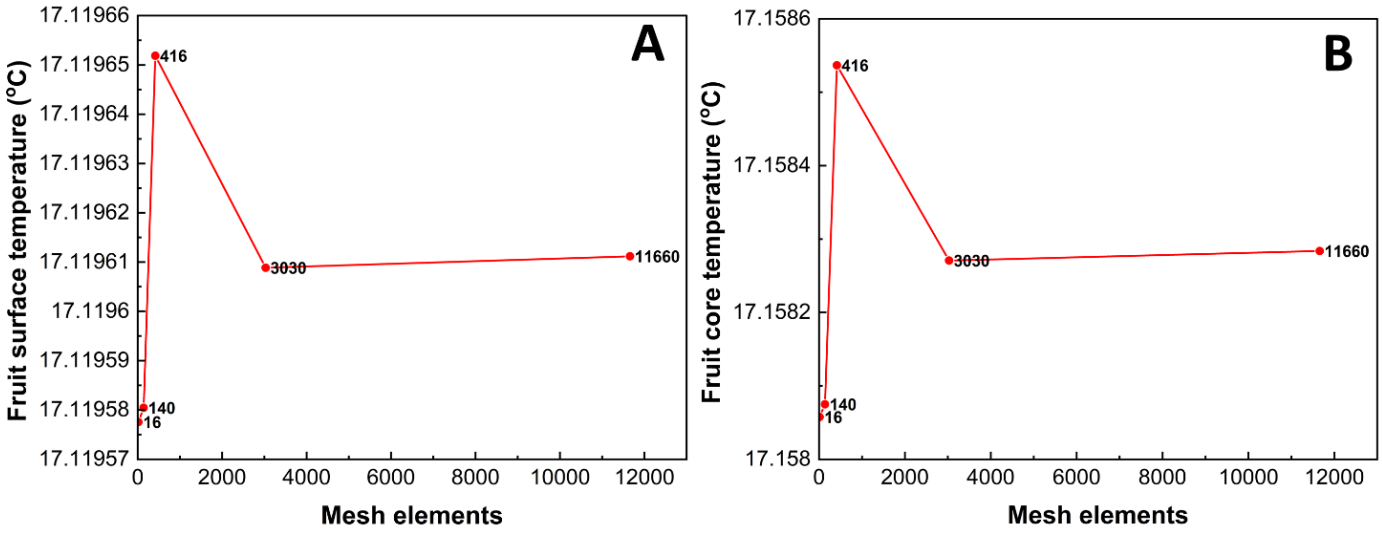

Figure S10. The Grid sensitivity analysis of extremely coarse (16 mesh elements), coarse (140 mesh elements), fine (416 mesh element), extra fine (base)(3030 mesh elements), and extreme fine grid (11660 mesh elements)for [A] the fruit surface temperature (°C) and [B] the fruit core temperature at 3.5 days after fruit set (anthesis).